MASS TRANSFER EVALUATION AND ANALYTICAL MODELING USING COMPOSITE HOLLOW FIBER MEMBRANE FOR SYNGAS FERMENTATION TO BIOFUELS

A DISSERTATION SUBMITTED TO THE GRADUATE DIVISION OF THE UNIVERSITY OF HAWAIʻI AT MĀNOA IN PARTIAL FULFILLMENT OF THE REQUIREMENTS FOR THE DEGREE OF

DOCTOR OF PHILOSOPHY

IN

MOLECULAR BIOSCIENCES AND BIOENGINEERING

DECEMBER 2012

By

Pradeep Chaminda Munasinghe

Dissertation Committee:

Samir Kumar Khanal, Chairperson
Scott Turn
Tao Yan
Reza Ghorbani
Roger Babcock

To my wife, daughter and parents

ACKNOWLEDGMENTS

I would like to extend my sincere gratitude and appreciation to my advisor Dr. Samir Kumar Khanal for his meticulous and scholarly guidance throughout the research. I am sure that this dissertation would not have been possible without his support, understanding, and encouragement during the study.

I would like to express my sincere appreciation to Drs. Scott Turn, Roger Babcock, Tao Yan and Reza Ghorbani for their willingness to serve on my dissertation examination committee and their advice on my research. I am thankful to Dr. Scott Turn for letting me use his analytical facility and Dr. Hong Cui for his support in gas chromatography analysis.

Appreciations also go to technical staff, Ryan Kurasaki, Charlie Nelson and Terrence Kai for their support in fabricating the bioreactors, and Karl Yanagihara for his technical support in gas chromatography. It was great to work with them. Further, I would also like to thank MBBE office staff including Joanne, Shan, Ardi, Karen and Loren for their friendships and administrative supports.

Thanks are also extended to my fellow lab mates, Devin, Saoharit (Pikky), Majda, Surendra, Rakshit, Matt, Ed and Zhen for their valuable discussion on research and course works, and above all their friendship during my 4 ½ years of study period in Hawaii.

Last but not the least, I extend my sincere gratitude to my wife, Pramoda, my loving daughter, Pranidhi, my parents, and sisters for their unconditional love, support, understanding and endurance throughout my study period. This dissertation is dedicated to my wife, daughter, and parents as a gift for their love and affection.

ABSTRACT

Mass transfer of synthesis gas (syngas) (primarily, carbon monoxide and hydrogen) in the aqueous phase is one of the major drawbacks associated with syngas fermentation. One way of addressing this issue is improving reactor design in order to achieve a higher volumetric mass transfer coefficient (k_La). The overall goal of this project was to evaluate the gas-liquid mass transfer of syngas constituents using various reactor configurations and analytical modeling of composite hollow fiber (CHF) membrane for potential applications in syngas fermentation.

Membranes are currently being employed extensively in water and wastewater treatment applications. There is a significant potential of using membranes in mass transfer for improving the efficiency of syngas fermentation. The novelty of this study is the evaluation of mass transfer and modeling of CHF membranes for syngas fermentation. Moreover, the dissolved CO in the aqueous phase was measured using a novel myoglobin (Mb) - protein bioassay.

The highest volumetric mass transfer coefficient (*Ka*) of 946.6±64.4 1/h for CO was observed using the CHF membrane module. Similarly, a maximum *Ka* value of 544.6±18.4 1/h for H_2 was obtained using the same reactor configuration. Moreover, model equations: $Sh=0.05\ P^{-0.22}Re^{0.24\ P^{0.48}}Sc^{0.33}$ and $Sh=0.21*10^{-2}*P^{0.49}Re^{0.45\ P^{0.25}}Sc^{0.33}$ for CO and H_2, respectively, were developed for scaling up the CHF membrane bioreactor. The validation of the model was conducted using polydimethyl siloxane (PDMSXA-2500 and PDMSXA-8300) membrane modules. An acceptable agreement between the overall volumetric mass transfer coefficients determined experimentally (Ka_{exp}) and using models (Ka_{model}), with a reliability of nearly, 85% was observed.

The study demonstrated the reliability of Mb-protein bioassay for CO analysis, and the potential of CHF membranes in improving the mass transfer of syngas in the aqueous phase for syngas fermentation. Further, the analytical modeling data will be useful for scaling-up syngas fermentation to industrial scale. Moreover, the developed models could be applied to examine the gas-liquid mass transfer coefficients in other systems such as wastewater treatment, syngas to methane, and syngas to carboxylic acid conversions.

TABLE OF CONTENTS

LIST OF TABLES

LIST OF FIGURES

Figures **Pages**

LIST OF ABBREVIATIONS

a: Membrane specific surface area (1/m)

A: Absorption value (unitless)

A_1: Membrane surface area (m^2)

C: Concentration of CO in water (mg/L)

C_0: Initial CO concentration in the liquid phase (mg/L)

C_i: Saturated CO concentration (mg/L)

C_p: Myoglobin-protein concentration (μM)

C^*: Liquid phase saturated gas concentration in equilibrium with the gas phase (mg/L)

d: Internal diameter of the membrane fibers (cm)

d_e: Effective diameter of the membrane (cm)

d_1: External diameter of the membrane fibers (cm)

d_2: Diameter of the membrane module (cm)

D: Diffusivity (m^2/s)

Gr: Graetz number (unitless)

Ka: Overall mass transfer coefficient (1/h)

H: Henry's law constant (atm)

k_La: Volumetric mass transfer coefficient (1/h)

l: Cell path length (cm)

L: Length of the membrane fibers (cm)

N: Number of fibers of a membrane module (unitless)

p: Partial pressure of gas above the aqueous phase (atm)

P: Inlet gas pressure (psig)

P_A: Partial pressure of a component gas (atm)

Pr: Percentile rank (unitless)

Q: Recirculation flow rate (L/min)

R^2: Correlation factor (unitless)

Re: Reynolds number (unitless)

SS: Percentage of CO saturated spectra obtained from SpectraSolve (%)

Sh: Sherwood number (unitless)

Sc: Schmidt number (unitless)

t: Time (s)

V: Volume of the reactor (L)

V_s: Sample volume in the cuvette (μL)

V_t: Total volume of the sample in the cuvette (μL)

v_L: Velocity through the membrane fibers (m/s)

x: Mole fraction (unitless)

α: Statistical significance (unitless)

ε_a: Molar absorptivity (1/μM.cm)

v: Kinematic viscosity (m^2/s)

CHAPTER 1

INTRODUCTION

1.1 Background

The total world demand for oil is projected to increase by 1% annually, mostly due to the increasing demand from emerging markets specially China and India (US EIA, 2012). Meanwhile, United States consumed nearly 18.8 million barrels per day (MMbd) of petroleum oil during 2011, becoming the largest oil consumer of the world. In 2011, U.S. imported nearly 45% of its total petroleum oil demand (8.4 MMbd) from foreign countries and approximately 50% of oil came from Persian Gulf and African countries which are politically unstable. This heavy dependence is causeing serious national security concerns and one of the major driving forces fueling research and development of sustainable biofuels in the United States (Gnansounou, 2010). Similarly, growing environmental concerns of greenhouse gas (GHG) emission (e.g., CO_2, CH_4, and N_2O) and its implications on climate change and rapid depletion of petroleum oil reserves are other driving forces responsible for renewable biofuel research.

Currently, biofuels are commercially produced from sugar, starch and oil-seed based feedstocks. For example, bioethanol is produced from corn starch in the United States, cassava starch in Thailand, and cane sugar in Brazil. Soybean, palm fruits, and rape and canola seeds are the common feedstocks for biodiesel production. The further expansion of biofuel production from many of these feedstocks, however, triggers debate on food/feed versus fuel. Thus, for sustainable biofuel production, non-food feedstocks should be used. Lignocellulosic biomass such as agri-residues (e.g., corn stover, and wheat and barley straws), agri-processing by-products (e.g., corn fiber, sugarcane bagasse, seed cake, etc.), and energy crops (e.g., switch grass, poplar, Napier grass, miscanthus, etc.) do not compete with food and feed, and is considered to be renewable feedstocks for biofuel production.

There are three major pathways for producing biofuels, namely carboxylic acid, biochemical and thermochemical pathways. Carboxylic acid pathway focuses on converting the biomass and other reduced carbon feedstocks into organic acids through anaerobic digestion. These low chain organic acids are then converted into the

corresponding alcohol-type fuels such as ethanol, and butanol. This pathway is still in its infant stage and yet to be optimized in terms of conversion efficiencies and product yields. During biochemical conversion, the biomass is subjected to acid, alkaline or steam explosion pretreatments to disrupt the cellulose-hemicellulose-lignin interactions. These pretreatments make the biomass more accessible to enzymes. The pretreated biomass is then subjected to enzyme hydrolysis to obtain fermentable sugars. The sugar-rich hydrolysate obtained is then fermented to biofuels (Heiskanen et al., 2007). Biochemical route, however, faces several challenges such as high pretreatment and enzyme costs, low fermentability of mixed sugar stream (5- and 6-carbon sugars), the generation of inhibitory soluble compounds (e.g., acetic acid, furfural, 5-hydroxymethyl-furfural, phenolic compounds, etc.), and the degradation of sugars during intense pretreatments. On the other hand, thermochemical pathway involves the gasification of biomass or other reduced carbon feedstocks such as coal or natural gas into synthesis gas or syngas in short (a mixture of CO, H_2 and CO_2), and then fermenting the syngas by microbial catalysts or chemical catalysts (Fischer-Tropsch (FT) method) to biofuels. The former, known as syngas fermentation, is considered to be more attractive due to several inherent merits over the biochemical approach and the FT method, such as (a) utilization of the whole biomass including lignin irrespective of the biomass quality; (b) elimination of complex pretreatment steps and costly enzymes; (c) higher specificity of the biocatalysts; (d) independence of the H_2:CO ratio for bioconversion; (e) aseptic operation of syngas fermentation due to generation of syngas at higher temperatures; (f) bioreactor operation at ambient conditions; and (g) no issue of noble metal poisoning. Biological catalysts (such as *Clostridium ljungdahlii*, *Clostridium autoethanogenum*, *Acetobacterium woodii*, *Clostridium carboxidivorans*, and *Peptostreptococcus productus*) are able to ferment syngas into liquid biofuels more effectively than the use of chemical catalysts (e.g., iron, copper or cobalt). The major drawbacks of the chemical catalytic process are the low specificity, high operating temperature and pressure, need of maintaining constant feed gas composition and high sensitivity to toxic gases.

Syngas can be produced from the gasification of several reduced carbon-rich feedstocks such as coal, oil shale, tar sand, and lignocellulosic biomass. Besides the

primary constituents, CO and H_2, gasification at a high temperature (750-800˚C) also produces other compounds such as methane (CH_4), carbon dioxide (CO_2), other higher hydrocarbons (e.g., C_2H_2, C_2H_4, and C_2H_6), particulate matter (e.g. tar, ash, and char particles), SO_x and NO_x, depending on the feedstocks. After gasification, the gas mixture passes through several gas clean-up unit operations including various types of filters and scrubbers to remove the impurities (both gaseous and particulate matter) from the mixture.

The major challenge of syngas fermentation is overcoming the gas-liquid mass transfer limitation of CO and H_2 in the aqueous phase. The stoichiometric substrate to product ratio of pure CO fermentation to ethanol is 6:1 (Vega et al., 1990), and with a significant amount of carbon and energy required to produce biomass and other metabolites, the actual ratio is even higher than stated above. Different approaches such as high gas and liquid flow rates, large specific gas-liquid interfacial areas, increased pressures, innovative impeller designs, modified fluid flow patterns, varying mixing times and speeds, and the use of micro-bubble dispersers have been examined to enhance gas solubility, thereby increasing the mass transfer, in the liquid phase. This strategy, however, is not economically attractive due to high energy costs. Additionally, higher agitation rates cause a low cell growth of the sensitive microorganisms resulting in low product yields. In order to achieve energy efficient mass transfer, innovative bioreactor configurations with optimized operational parameters should be investigated for syngas fermentation.

The gas-liquid volumetric mass transfer coefficient (k_La) which represents the hydrodynamic conditions in a reactor can be used as a reliable parameter to examine the effective mass transfer rate. To date, a significant number of studies have been conducted to examine mass transfer rate using various reactor configurations, but few studies examined the potential for scale-up. Bredwell et al. (1999) reported maximum k_La values of 75, 190 and 335 1/h for H_2 gas in a continuous-stirred tank reactor, stirred tank coupled with micro-bubble sparger and a trickle bed reactor, respectively. The authors used a mixed culture of sulfate-reducing bacteria (SRB) and an agitation speed of 300 rpm in their study.

The use of composite hollow fiber (CHF) membranes in syngas fermentation is an innovative approach which offers several advantages over the conventional bioreactor configurations. Three layered, CHF membranes manufactured from hydrophobic material such as polyethylene can be used effectively to enhance the gas-liquid mass transfer in aqueous phase. Even though this technique has not been adopted exclusively in syngas fermentation, it has been used extensively in hydrogen and oxygen mass transfer both in water and wastewater treatment applications (Lee and Rittmann, 2001). Since these CHF membranes consist of a non-porous ultra thin layer (< 1μm), it prevents the permeation of liquids on the non-pressurized side, allowing only the gases to pass through and increasing the durability of the membrane fibers. In these modules, higher gas saturation levels can be achieved by increasing the inlet gas pressure (Ahmed et al., 2004). Moreover, the scaling up of a system with CHF membrane bioreactors is easier than the conventional reactors due to the compact and modular nature of the membrane bioreactors. Therefore, it is important to develop analytical models using lab-scale CHF membrane reactors, in order to successfully scale-up the technology. This study was the first to evaluate the potentials of CHF membrane module for mass transfer of syngas.

The efficacy of syngas fermentation is evaluated primarily based on the mass transfer rate of CO into the aqueous phase. All syngas fermentation studies reported so far employs Henry's law and the CO partial pressure in the head space to indirectly calculate the dissolved CO in the aqueous phase. Such an approach is not only tedious, but also time consuming and expensive. In this study, we employed a new method known as myoglobin (Mb)-protein bioassay for the determination of CO in aqueous samples. The Mb-protein bioassay is a much simpler, faster and cheaper method than gas chromatograph equipped with thermal conductivity detector (GC-TCD) analysis currently used for the determination of CO concentrations in the aqueous phase (Kundu et al., 2003). To our knowledge, this is the first study that experimentally confirms that the Mb-protein bioassay is an accurate, reliable and simpler method compared to the GC-TCD method for aqueous phase CO determination in syngas-to-biofuel conversions.

1.2 Objectives of the Study

The overall goal of this research was to evaluate the gas-liquid mass transfer using different reactor configurations and analytical modeling of CHF membrane bioreactor for syngas fermentation. The specific objectives of this research include the following:

1) Develop a correlation between the myoglobin (Mb)-protein bioassay and the gas chromatography (GC) method for CO;

2) Examine the volumetric mass transfer coefficients (k_La) of CO using different reactor configurations;

3) Develop and test an analytical model for CO and H_2 mass transfer using composite hollow fiber (CHF) membrane module.

1.3 Scope of the Study

The study focused on comparing the k_La values of different reactor configurations including a column diffuser, a 20-μm bulb diffuser, gas sparger, gas sparger with mechanical mixing, submerged composite hollow fiber (CHF) membrane bioreactor, air-lift combined with a 20-μm bulb diffuser, air-lift combined with a single gas entry point and a CHF membrane bioreactor (placed separately from the main reactor). During laboratory scale syngas fermentation experiments *C. carboxidivorans* was used as the microbial catalyst. The analytical model was developed using CHF membrane bioreactor for both CO and H_2. In order to validate the models developed, polydimethyl siloxane (PDMSXA-2500 and PDMSXA-8300) membrane modules were used.

CHAPTER 2

LITERATURE REVIEW

2.1 Synthesis Gas Fermentation

2.1.1 Background

World's use of petroleum and other liquid fuels (non petroleum derived fuels such as ethanol, biodiesel, coal-to-liquid and natural gas-to-liquid fuels) is expected to grow from 85.7 million barrels per day in 2008 to 97.6 million barrels per day in 2020, and 112.2 million barrels per day in 2035. Further, liquid fuels remain as the primary energy source for both transportation and industrial sectors. According to US EIA (2012), liquid fuel production (including both conventional and nonconventional liquid fuel supplies such as oil sand, biofuels, coal-to-liquid, natural gas-to-liquid) is expected to increase by a total of 26.6 million barrels per day from 2008 to 2035 to meet the rising demand of growing world population. The United States, being the largest importer of the petroleum fuels, is heavily dependent on imports thereby weakening national security. The growing concerns of climate change associated with energy-derived greenhouse gas emissions, and rapidly depleting petroleum based resources are key factors that play an important role in seeking renewable energy sources such as biofuels.

Biofuels are commercially produced from sugar-based (sugar beet, sugar cane), starch-based (corn, cassava) or oil based (soybean, rapeseed, palm fruits) feedstocks. Since all of these feedstocks are food/feed based crops, further expansion of biofuel production from these feedstocks leads to the concerns over food/feed versus fuel. Therefore, currently, non-food/feed based feedstocks, such as lignocellulosic biomass, and abundantly available resources such as coal, natural gas, oil shale are considered to be the potential feedstocks for liquid fuel production.

2.1.2 Biofuel production pathways

There are three major pathways of producing biofuels from various feedstocks such as biomass, coal or natural gas, namely, carboxylic acid, thermochemical and biochemical pathways (Fig. 2.1). During carboxylic acid pathway, the feedstocks are converted into their respective carboxylic acids which can then be converted into biofuels through thermochemical pathway. In the case of biochemical pathway, the feedstock is

subjected to acid, base or steam/hot water washing pretreatment followed by enzyme hydrolysis to release fermentable sugars for subsequent biofuel production. The major issues with biochemical pathway are low overall sugar release, cost of pretreatment and enzymes. In thermochemical pathway, feedstocks (biomass or other reduced carbon feedstocks) are gasified into a gas mixture (consisting of mainly CO, CO_2 and H_2) known as synthesis gas or syngas in short. The obtained gas mixture can be converted into biofuels either by chemical catalysts (known as Fischer-Tropsch (FT) synthesis) or by microorganisms (known as syngas fermentation). FT synthesis has its own limitation due to the high catalysts cost and noble metal poisoning. However, syngas fermentation overcomes nearly all of the shortcomings of the FT synthesis. Further, syngas fermentation is considered to be more attractive due to the inherent merits such as higher specificity, low operational cost, independent of CO: H_2 ratio for bioconversion, aseptic operation, and ambient operational conditions of the bioreactors.

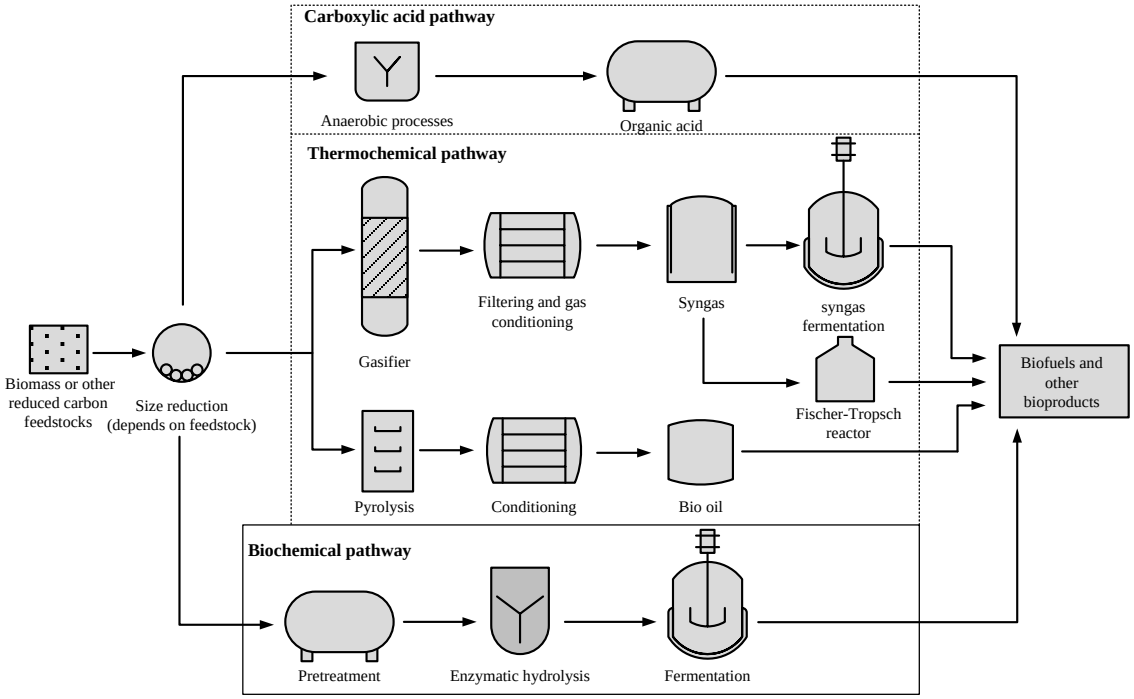

Note: Syngas can be produced from other feedstocks such as coal or natural gas

Figure 2.1. Different pathways of biofuel production

2.1.3 Syngas conversion to ethanol

The catalytic conversion of syngas to hydrocarbons and alcohol fuels by Fisher-Tropsch (FT) synthesis was invented by German scientists Franz Fisher and Hans Tropsch in 1923 (Demirbas, 2007). During energy embargo of 1970's, the conversion of syngas to higher alcohols by FT synthesis appeared as a potential alternative to petroleum fuel (Stelmachowski and Nowicki, 2003). In 1987, *C. ljungdahlii*, a rod shape, gram-positive anaerobic bacteria was discovered which was found to have an ability to ferment carbon monoxide and hydrogen into ethanol and acetic acid (Lynd, 2008). Since then, there has been significant development in syngas fermentation research, especially in process microbiology with discovery of over dozens of new species and process engineering such as new reactor design for improved mass transfer among others (Lynd, 2008).

Gasification of lignocellulosic biomass at a high temperature (750 to 800˚C) produces a gas mixture containing carbon monoxide (CO), hydrogen (H_2), methane (CH_4), nitrogen (N_2), carbon dioxide (CO_2) and some higher hydrocarbons commonly known as producer gas (Datar et al., 2004). The overall gasification process is endothermic, that is, it requires heat-energy input to drive the process. The composition of producer gas depends on the types of gasifier and biomass, and the gasification conditions among others. Table 2.1, summarizes the constituents of the gas produced from different gasifiers under different gasification conditions. The synthesis gas predominantly contains H_2 and CO, and is commonly known as syngas in short. After gasification, the syngas mixture passes through a series of filters to remove undesirable pollutants such as tar and solid particles. The purified syngas is then converted into liquid fuels by microbial catalysts.

Table 2.1. Gas compositions of different gasification processes

Gas constituents \ Gasifier types	Fluidized bed air blown	Updraft air blown	Downdraft oxygen blown	Fluidized bed (switchgrass)	Fluidized bed (bark)	Fluidized bed (coal)
N_2 (%)	50	53	3	57	43	1
CO (%)	14	24	48	15	20	67
CO_2 (%)	20	9	15	17	13	4
H_2 (%)	9	11	32	5	20	24
CH_4 (%)	7	3	2	6	4	0
H_2S (%)	n/a	n/a	n/a	n/a	Very low	1
Tars (g/m^3)	<10	>10	1	<1	<1	0
H_2O (%)	n/a	n/a	n/a	n/a	Dry	3
Dust	High	Low	Low	n/a	n/a	n/a
References	Bridgwater, 1995	Bridgwater, 1995	Bridgwater, 1995	Datar et al., 2004	Subramani and Gangwal, 2008	

2.1.4 Metabolic pathways of syngas fermentation

Syngas fermenting microorganisms such as *C. ljungdahlii*, *C. carboxidivorans, C. autoethanogenum, C. ragsdalei, Butyribacterium methylotrophicum* follow the acetyl-CoA pathway (also known as Wood-Ljungdahl pathway) to produce biofuels (Fig. 2.2) (Henstra et al., 2007). Microorganisms that produce the intermediate acetyl-CoA from carbonyl or carboxyl precursors are known as acetogens (Brown, 2006). Though, many acetogenic microbes produce acetates from alcohols and fatty acids, some are capable of producing organic acids and alcohols using CO_2 and H_2 (autotrophic acetogens) or CO (unicarbonotrophic acetogens) as their substrates (Grethlein and Jane, 1993).

Figure 2.2 shows the simplified acetyl-CoA pathway leading to the production of bio-based products such as ethanol and acetic acids from syngas. The essential reducing equivalents (-CO, -CoA, -Co-CH_3) are produced from H_2 and CO by hydrogenase and CO dehydrogenase (CODH) enzymes, respectively (Fischer et al., 2008). In addition, the bifunctional CODH enzyme produces a carbonyl group from the reaction of carbon dioxide and water (Henstra et al., 2007). The produced reducing equivalents are then converted to acetyl-CoA by acetyl-CoA synthase (ASC) complex.

During the metabolic pathway, intermediate acetyl-CoA performs two major roles - it acts as a precursor for the cell macromolecule (anabolism), and it serves as an energy source (catabolism). During the anabolic pathway, acetyl-CoA is carboxylated into pyruvate and then gets converted into phosphoenolpyruvate which is considered to be an intermediate to produce cell materials (Mohammadi et al., 2011). On the other hand, during the catabolic pathway, acetyl-CoA gets converted to acetate via formation of acetyl-phosphate as the intermediate. Conversion of acetyl-CoA to acetate and ATP is carried out during the growth phase, whereas the alcohol and NADH production takes place in non-growth phase of the metabolism. In this case, conversion of acetyl-CoA to alcohols is carried out via acetaldehyde (CH_3CHO) in the presence of acetaldehyde dehydrogenase. Even though the biochemistry of the pathway is described in detail in numerous excellent reviews (Ragsdale and Pierce, 2008; Wood, 1992), the energy conservation associated with the pathway has yet to be examined (Kopke et al., 2011).

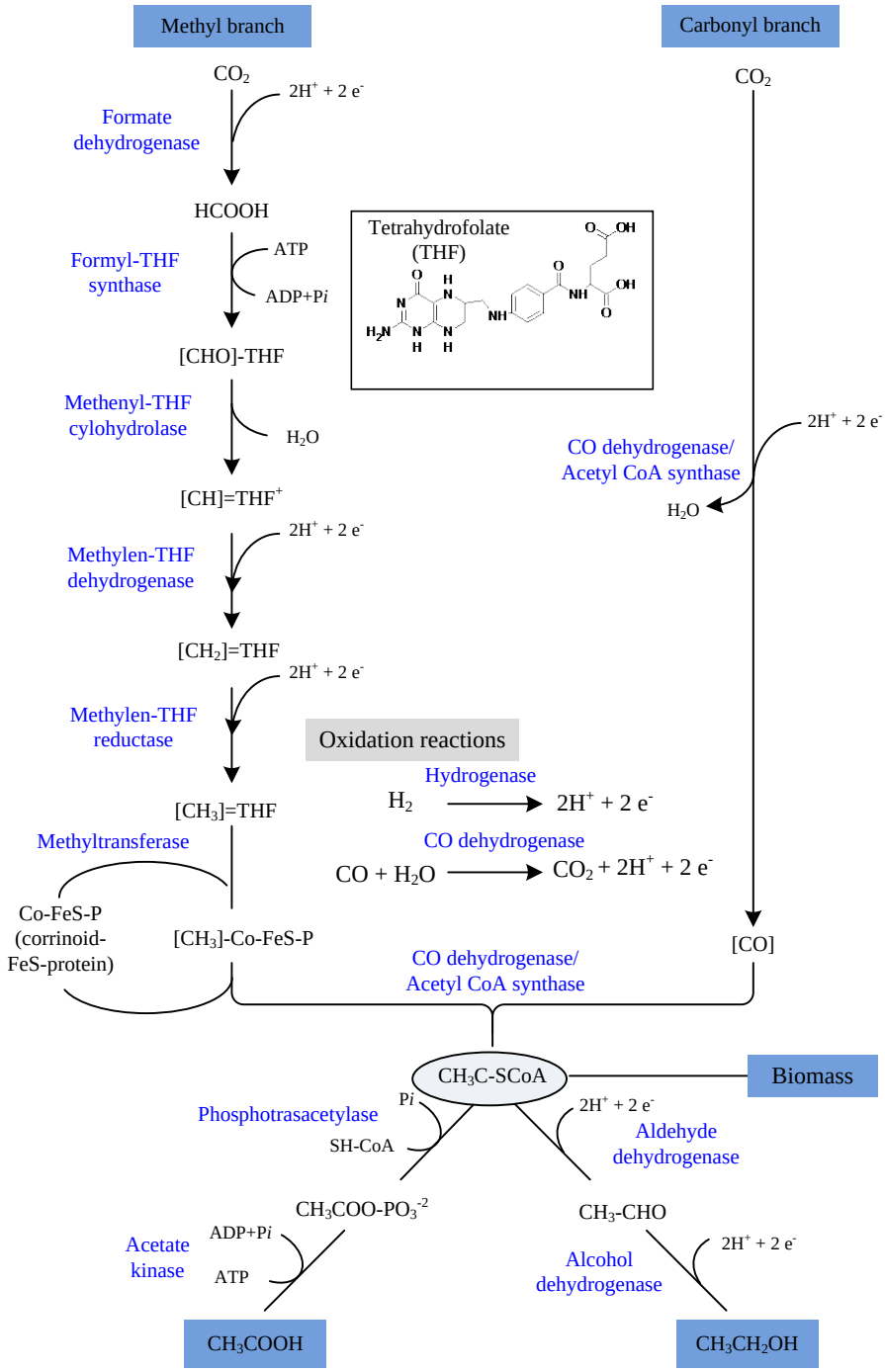

Co: A corrinoid protein (Methyl group carrier)

Figure 2.2. Acytyl-CoA (or Wood-Ljungdahl) pathway for acetogenic microorganisms (modified from Kopke et at., 2011)

2.1.5 Biochemical reactions

Acetic acid (CH_3COOH) and ethanol (C_2H_5OH) are the two major products from syngas fermentation. Eqs. (2.1) to (2.4) show the four basic reactions producing acetic acid and ethanol (van Kasteren, 2006). In this case, the gaseous substrates CO and H_2 follow the acetyl-CoA pathway to produce acetic acid and ethanol under strict anaerobic conditions.

$$6CO + 3H_2O \longrightarrow C_2H_5OH + 4CO_2 \qquad \Delta G° = -216.0 \text{ kJ/mol} \quad (2.1)$$

$$6\,H_2 + 2\,CO_2 \longrightarrow C_2H_5OH + 3H_2O \qquad \Delta G° = -97.1 \text{ kJ/mol} \quad (2.2)$$

$$4CO + 2H_2O \longrightarrow CH_3COOH + 2CO_2 \qquad \Delta G° = -135.0 \text{ kJ/mol} \quad (2.3)$$

$$6\,H_2 + 2\,CO_2 \longrightarrow CH_3COOH + 2H_2O \qquad \Delta G° = -54.8 \text{ kJ/mol} \quad (2.4)$$

From eq. (2.1), it is clear that about one third of the carbon from CO is utilized in the product yield. The overall ethanol production, combining eqs. (2.1) and (2.2), reveals that two thirds of the carbon from CO is converted to ethanol. During the acetyl-CoA pathway, hydrogen provides the required reducing equivalents and electrons when hydrogenase enzyme is present in the fermentation media (eq. (2.5)).

$$H_2 \longrightarrow 2H^+ + 2\,e^- \qquad (2.5)$$

If the hydrogenase enzyme is inhibited or hydrogen is not present in the fermentation broth, the required electrons are obtained from CO in the presence of CODH enzyme. In other words, CO is used in supplying electrons, rather than in the biofuel production. This obviously results in a drastic reduction in biofuel yields. It is therefore, important to maintain adequate concentrations of both hydrogen and CO during syngas fermentation.

2.1.6 Microbiology of syngas fermentation

Currently known microorganisms capable of fermenting syngas into ethanol and other bioproducts are predominantly mesophilic (Table 2.2). The most favorable operational temperature for mesophilic microorganisms is between 37 and 40ºC where as for thermophilic, the temperature varies between 55 and 80ºC. Some thermophilic microbes however, can operate at a higher temperature than reported above (Henstra et

al., 2007). Mesophilic microorganisms, e.g., *C. aceticum, Acetobacterium woodii, C. carboxidivorans* and *C. ljungdahlii* have been widely studied in syngas fermentation (Younesi et al., 2005). Since, syngas exits the gasifier at a very high temperature, it has to be cooled down before introducing into the fermentor. The released excess heat can be recovered by coupling the process with a heat recovery system.

The most favorable pH range for efficient microbial activity varies between 5.8 and 7.0 depending on the species. For example, the optimal pH was reported around 5.8 to 6.0 for *C. ljungdahlii*. An ethanol concentration as high as 48 g/L was obtained in a continuous-flow system at a low pH of 4.0 to 4.5, coupled with a nutrient-limited environment using *C. ljungdahlii* (Klasson et al., 1993). In a separate study, a mesophilic bacterium, *C. carboxidivorans* (or P7), was used in syngas fermentation in a continuously-operated bubble column reactor at pH of 5.75 (Rajagopalan et al., 2002). The authors claimed that the bacterial strain P7 has a higher ethanol selectivity and yield on CO than *C. ljungdahlii* thereby resulting in a higher ethanol production.

The use of thermophiles in syngas fermentation is in an infant stage. There are some merits of evaluating syngas fermentation at thermophilic conditions as the syngas exits the gasifier at a high temperature between 700 to 800˚C. Thermophilic microbes such as *Carboxydocella sporoproducans, Desulfotomaculum carboxidivorans, Moorella thermoacetica* and *M. thermoautotrophica* were found to grow on CO (Table 2.2). Until recently, there were no thermophiles capable of converting gaseous substrates such as CO and H_2 into organic compounds.

Table 2.2. Frequently used mesophilic and thermophilic microorganisms and their optimum growth conditions

Species	T_{opt} (°C)	pH_{opt}	Products	References
Mesophilic microorganisms				
A. woodii	30	6.8	Acetate	Genthner and Bryant, 1987
B. methylotropphicum	37	6.0	Acetate, butyrate, ethanol, butanol	Grethlein et al., 1991; Lynd et al., 1982
C. acetobutylicum	37	4.5	Acetate, butyrate, ethanol, butanol	Worden et al., 1991
C. aceticum	30	8.5	Acetate	Sim et al., 2007
C. autoethanogenum	37	5.8-6.0	Acetate, ethanol	Abrini et al., 1994
C. carboxidivorans	38	6.2	Acetate, ethanol, butyrate, butanol	Liou et al., 2005
C. leatocellum SG6	35	7-7.2	Acetate, lactate, ethanol	Ravinder et al., 2001
C. ljungdahlii	37	6.0	Acetate, ethanol	Tanner et al., 1993
Eubacterium limosum	38-39	7.0-7.2	Acetate	Genthner and Bryant, 1987
Mesophilic bacterium P7	37	5.7-5.8	Acetate, ethanol, butyrate, butanol	Rajagopalan et al., 2002
Oxabactor pfennigii	36-38	7.3	Acetate, n-butyrate	Krumholz and Bryant, 1985
Peptostreptococcus productus	37	7.0	Acetate	Lorowitz and Bryant, 1984
Thermophilic microorganisms				
Carboxydocella sporoproducens	60	6.8	H_2	Slepova et al., 2006
C. thermocellum	60	7.5-6.0	Acetate	Florenzano and Poulain, 1984
Desulfotomaculum thermobenzoicum subsp. Thermosyntrophicum	55	7.0	Acetate,H_2S	Parshina et al., 2005
M. thermoacetica (Clostridium thermoaceticum)	55	6.5-6.8	Acetate	Daniel et al., 1990
M. thermoautotrophica	58	6.1	Acetate	Savage et al., 1987

2.2 Reactor Design for Syngas Fermentation

Both batch and continuous-flow bioreactors have been examined for syngas fermentation. In batch reactors, the gaseous substrate is introduced into the bioreactor and fermented in a closed system. The gaseous substrate is supplied continuously. The liquid samples are withdrawn at a selected time during fermentation. Vega et al. (1990) examined the kinetic parameters through a series of batch experiments. Traditionally, a continuous stirred-tank reactor (CSTR) was examined in syngas fermentation. Bubble column reactors, monolithic biofilm reactors, trickling bed reactors and microbubble dispersion stirred-tank reactors are some of the other common bioreactors which have been studied under both continuous and batch-mode operations. Different types of reactor configurations employed in syngas fermentation are briefly discussed here.

2.2.1 Continuous stirred-tank reactor (CSTR)

The continuous stirred-tank reactor (Fig. 2.3(A)) is the most common bioreactor employed in syngas fermentation. In CSTRs, gaseous substrate is injected continuously, and a liquid nutrient (culture media) is fed into the bioreactor to supplement nutrients for microbial metabolism (Klasson et al., 1992; Vega et al., 1990). The fermentation product is drawn from the system at the same rate as the feed. A higher level of agitation or mixing is maintained in the reactor by baffled impellers to enhance the mass transfer between the substrate and the microbes. Higher rotational speeds of the impellers tend to break the gas bubbles into finer ones thereby making the gaseous substrate more accessible to the microbes. In addition, the slow rising velocity of the finer bubbles leads to longer gas retention in the aqueous medium, which results in higher mass transfer rates.

2.2.2 Bubble column reactor

Bubble column reactors (Fig. 2.3(B)) are designed mainly for industrial applications with large working volumes. Higher mass transfer rates and low operational and maintenance costs are the primary merits of this system, while back-mixing and coalescence are considered to be the major drawbacks of bubble column reactors (Datar et al., 2004).

2.2.3 Monolithic biofilm reactor

In monolithic biofilm reactors, the gaseous substrate is allowed to pass through a bed of carrier media. The microbes grow on the media as biofilm. During the operation, attached microorganisms in the biofilm utilize the gaseous substrates to produce ethanol, acetic acid and other end-products. The monolithic biofilm reactors are operated under atmospheric pressures, making the process more economically viable.

2.2.4 Trickle-bed reactor

A trickle-bed reactor (Fig. 2.3(C)) is a packed bed, continuous reactor in which the liquid culture flows down through packing media. The syngas is allowed to move either downward (co-current) or upward (counter-current) direction. Since these types of reactors do not require mechanical agitation, the power consumption of trickle-bed reactors is lower than the CSTR (Bredwell et al., 1999).

2.2.5 Microbubble dispersion stirred-tank reactor

A microbubble dispersion stirred-tank reactor (Fig. 2.3 (D)) is a stirred-tank equipped with a microbubble sparger. Bredwell et al. (1999) found that the mass transfer of the system increased in two ways. Firstly, decreasing bubble sizes cause internal pressure increase, leading to an increase in the driving force. Secondly, the steady state liquid phase concentration gradient at the surface of the bubble is inversely proportional to the diameter. In other words, the flux increases as the diameter of the bubble decreases.

2.2.6 Membrane-based system

Composite hollow fiber (CHF) membranes can be used effectively to facilitate the mass transfer in aqueous culture media. Even though, this technique has not been adopted exclusively in syngas fermentation, it was examined for hydrogen and oxygen transfer in water treatment applications (Lee and Rittmann, 2001; Nerenberg and Rittmann, 2004). In the CHF membrane reactors, syngas is diffused through the walls of membranes without forming bubbles. The microbial community in the reactor uses these diffused gases to produce biofuels. This innovative approach offers significant advantages in achieving a higher yield and reaction rate, and a higher tolerance to toxic compounds present in syngas (tar, acetylene, NO_x, O_2).

Moreover, these CHF membrane bioreactors can be operated under high pressure with higher mass transfer rates and reduced reactor volumes. Microorganisms which can tolerate high pressures can be utilized in the fermentation process as microbial catalysts (Madigan et al., 1997).

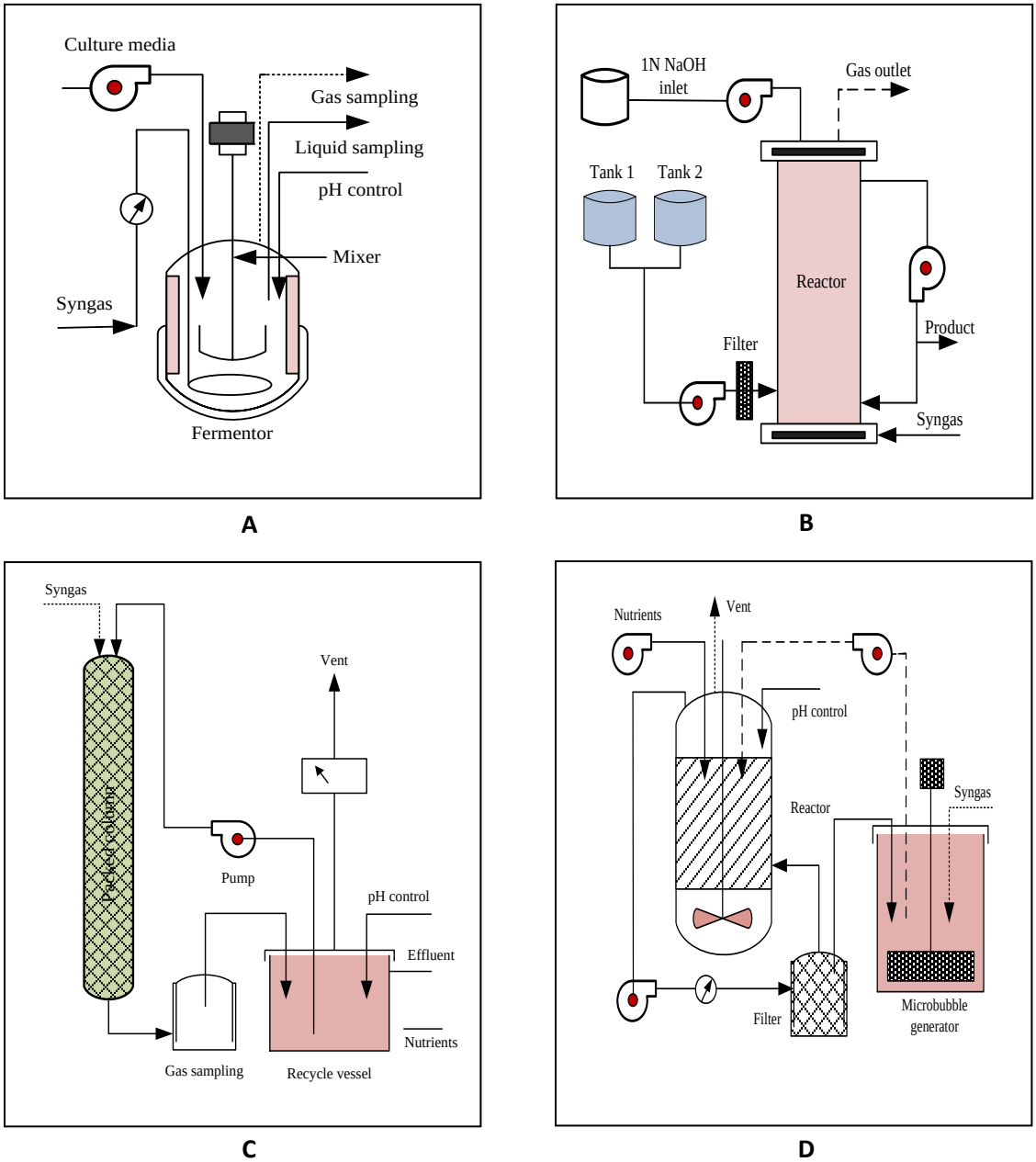

Figure 2.3. Various reactor configurations used in syngas fermentation (A) Continuous stirred-tank reactor (CSTR); (B) Bubble column reactor; (C) Trickle-bed reactor; (D) Microbubble dispersion stirred-tank reactor

2.3 Factors Affecting Syngas Fermentations

2.3.1 Inhibitory compounds

Biomass-derived syngas often contains additional constituents such as ethylene (C_2H_4), ethane (C_2H_6), acetylene (C_2H_2), tar, ash, char particles and gases containing sulfur and nitrogen (Ahmed et al., 2006; Bridgwater, 1994; Haryanto et al., 2009). These impurities in the syngas affect the efficiency of the fermentation process by potential scaling in pathways, and inhibiting the microbial catalysts resulting in low cell growth and product yield. Datar et al. (2004) reported cell dormancy, hydrogen uptake shutdowns and a shift in pathways from acidogenesis to solventogenesis and vice versa, when the syngas was used without conditioning. Ahmed and Lewis (2007) was able to overcome cell dormancy by introducing a 0.025 µm filter to remove tar, ash and other particulate matter from the biomass-derived producer gas. Nitrous oxide (NO) was found to be a potential inhibitor of hydrogenase enzyme activity, which reduced the available carbon for product formation (Ahmed and Lewis, 2007). The inhibitory effects of NO on syngas fermentation can be eliminated by improving the gasification efficiency or by scavenging it using agents such as, sodium hydroxide, potassium permanganate or sodium hypochlorite (Brogren et al., 1997; Chu et al., 2001). Klasson et al. (1993) studied the sulfur gas tolerance of *C. ljungdahlii*. The authors found that the growth of *C. ljungdahlii* was not significantly affected by H_2S concentrations as high as 5.2% (v/v).

Turn et al. (2003) examined the feasibility of improving fuel characteristics of sugarcane bagasse by introducing pretreatment methods such as milling and leaching. After an initial milling pretreatment, the N, S and Cl contents of the sugarcane bagasse were reduced to 0.42, 0.14 and 0.25% (dry wt. basis) from their initial values of 0.48, 0.22 and 0.65%, respectively. Further, the combined pretreatment of milling-leaching-milling reduced the N, S and Cl contents to 0.35, 0.04 and 0.04%, respectively, from their initial values. Such pretreatments could reduce the production of SO_x and NO_x during biomass gasification.

2.3.2 Mass transfer

Gas-liquid mass transfer is a rate-limiting step in syngas fermentation process (Klasson et al., 1993; Worden et al., 1991). Mass transfer limitations are inevitable at

several points of the diffusion process including the transport of gaseous substrate into gas-liquid interface, its transport into culture media (aqueous phase), the transport of the mixed gases into the stagnant liquid layer around the microbes, and the diffusion of the transported gaseous substrate into the microbial cells. The gas-liquid interface mass transfer is the major resistance for gaseous substrate diffusion.

Diffusion limitations of a gaseous substrate into the culture media results in low substrate uptake by microbes and thus, leads to low productivity. Therefore, knowledge of mass transfer coefficients would be more advantageous to understand the rate of mass transfer. The mass transfer coefficient (k_L) (m/s) for a slightly soluble gaseous substrate can be determined using eq. (2.6) (Klasson et al., 1992).

$$\frac{1}{V_L}\frac{dN_S^G}{dt} = \frac{k_L a}{H}\,(P_S^G - P_S^L) \tag{2.6}$$

Where, N_S^G (mol) is the molar substrate transferred from the gas phase

V_L (L) is the volume of the reactor

P_S^G and P_S^L (atm) are the partial pressures of the gaseous substrate in gas and the liquid phase, respectively

H (L.atm/mol) is the Henry's law constant

a (m^2/L) is the gas-liquid interface surface area per unit volume

The difference in the partial pressures of the gaseous substrate $(P_S^G - P_S^L)$ is the driving force for mass transfer and thus controls the solubility of the substrate. High pressure operation improves the solubility of the gas in aqueous phase. However, at higher concentrations of gaseous substrates, especially CO, anaerobic microorganisms are inhibited. Therefore, the determination of a correlation between the substrate diffusion and the specific substrate uptake rate (q_S) (1/h) is important in order to evaluate the process kinetics (eq. (2.7)).

$$q_S = \frac{q_m\, P_S^L}{K'_p + P_S^L + (P_S^L)^2/W'} \tag{2.7}$$

Where, q_m (1/h), W' (atm) and K'_p (atm) are empirical constants. Furthermore, Q_S (mg/L.h), the substrate uptake rate, can be written as $Q_S = q_S X$; where X (mg/L) is the microbial cell concentration. By analyzing the above equation, it can be concluded that the operating pressure of the reactor is inversely proportional to the cell concentration (Vega et al., 1990).

Many earlier studies examined mass transfer using different bioreactor configurations (Bouaifi et al., 2001; Bredwell et al., 1999). Table 2.3 summarizes the volumetric mass transfer coefficients ($k_L a$) for different reactor configurations under various hydrodynamic conditions.

The most common approach for improving the mass transfer in CSTRs is to increase the agitation speed of the impeller (Bredwell et al., 1999). By implementing this strategy, it is possible to obtain smaller bubbles sizes, thus increasing the gas-liquid interfacial area for efficient mass transfer. However, the high energy requirement of the system greatly reduced its economic viability in industrial-scale syngas fermentations. Consequently, other reactor configurations such as trickling bed reactors, air-lift reactors (Bredwell et al., 1999) and bubble column reactors (Bouaifi et al., 2001; Datar et al., 2004) have been examined for an efficient mass transfer. Bouaifi et al. (2001) compared the mass transfer rates between stirred-tank and bubble column reactors and found that the $k_L a$ obtained for the bubble column reactor was higher than that of the stirred-tank reactor. This was mainly due to higher interfacial area obtained in the bubble column. In a separate study, Bredwell and Worden (1998) examined the hydrodynamic and mass transfer properties of microbubble dispersions in a bubble column reactor. The authors concluded that the axial mixing of the microbubble dispersion was considerably less than that of the conventional bubble column reactors.

2.3.3 Reactor configuration

Reactor configuration is closely related to the gas-liquid mass transfer efficiency. Thus, reactor design plays an important role in syngas fermentation. High mass transfer rates, low operation and maintenance costs and easy scale-up are some of the key parameters for designing an efficient bioreactor system. Similarly, the bioreactor size greatly depends on the rate of mass transfer for sparingly soluble gases (Vega et al.,

1990). CSTRs are the most commonly used bioreactors for syngas fermentation. Bubble columns, packed bubble columns, trickle-bed reactors and microbubble sparged reactors are some of the other configurations which have been examined for syngas fermentation.

2.3.4 Temperature

Temperature effects are important for two reasons. Firstly, it affects the microbial growth and substrate utilization in syngas fermentation and secondly, it affects the solubility of gaseous substrate in aqueous medium. The most favorable growth temperature range for mesophilic microorganisms is from 37 - 40ºC, while for thermophilics, it ranges between 55 - 80ºC. Although, thermophilic operations at a high temperature result in a reduction in gas solubility in the culture medium, it increases the rate of mass transfer of the process due to low viscosity.

2.3.5 pH

pH is an important parameter for the optimal activity of microbial catalysts. The optimum pH for syngas-fermenting microbes varies between 5.5 and 7.5 depending on the species. For example, *C. ljungdahlii* has an optimum pH of 5.8 to 6.0. The optimum growth pH for some of the commonly used mesophilic and thermophilic microorganisms are given in Table 2.2.

2.3.6 Growth media

Growth media provides the microbes with all essential nutrients including minerals, trace elements, vitamins and reducing agents for their maximal growth. The selection of the growth media depends on the selected species and the targeted end products. For example, American Type Culture Collection (ATCC) medium 1754 (PETC medium) is used as the growth medium for *C. ljungdahlii*, *Acetobacterium* medium (ATCC medium1019), and *Thermoanaerobacter ethanolicus* medium (ATCC medium1190) are some of the frequently used growth media.

Table 2.3. Volumetric mass transfer coefficients (k_La) in various reactor configurations and hydrodynamic conditions

Reactor configurations	N^* (rpm)	Microorganisms	Gas	k_La (1/h)	References
Trickle bed	n/a	n/a	Syngas	22	Cowger et al., 1992
Continuous stirred tank	n/a	n/a	Syngas	38	
Continuous stirred tank	200	*B. methylotrophicum*	CO	14	Bredwell et al., 1999
Continuous stirred tank	300	SRB** mixed culture	Syngas	31 for CO, 75 for H_2	
Continuous stirred tank	300	*C. ljungdahlii*	Syngas	35 for CO	
Continuous stirred tank	300	*R. rubrum*	Syngas	28 for CO	
Continuous stirred tank	450	*R. rubrum*	Syngas	101 for CO	
Stirred tank - microbubble sparger	200	*B. methylotrophicum*	CO	91	
Stirred tank - microbubble sparger	300	SRB** mixed culture	Syngas	104 for CO, 190 for H_2	
Packed bubble column	n/a	*R. rubrum*	Syngas	2	
Trickle bed	n/a	*R. rubrum*	Syngas	56	
Trickle bed	n/a	SRB** mixed culture	Syngas	121 for CO, 335 for H_2	
Trickle bed	n/a	*C. ljungdahlii*	Syngas	137 for CO	
Batch stirred tank	n/a	*P. productus*	CO	7	Vega et al., 1990
Stirred tank	300	*C. ljungdahlii*	CO	15	Klasson et al., 1993
Stirred tank	400	*C. ljungdahlii*	CO	22	
Stirred tank	500	*C. ljungdahlii*	CO	23	
Stirred tank	600	*C. ljungdahlii*	CO	24	
Stirred tank	700	*C. ljungdahlii*	CO	36	
Bubble column	n/a	n/a	CO	72	Chang et al., 2001
Stirred tank	400	n/a	CO	76	Riggs and Heindel, 2006
Stirred tank	500	*R. rubrum*	Syngas	72	Younesi et al., 2008

N^*: Agitation speed; SRB**: Sulfate-reducing bacteria

2.3.7 Types of microorganisms

The selection of appropriate microbes for efficient syngas fermentation is a challenging task. Strict mesophilic anaerobes such as *C. ljungdahlii*, *C. aceticum, A. woodii, C. autoethanogenum,* and *C. carboxidivorans* are frequently being used in syngas fermentation (Klasson et at., 1992; Rajagopalan et al., 2002; Younesi, at al., 2005). In addition, the isolation and engineering of new microbial species, which are more productive and robust, need to be developed.

2.4 Current Developments in Syngas Fermentation

2.4.1 Biorefinery concept

According to the Biomass Research and Development Technical Advisory Committee Report (2002) published by the U.S. Department of Energy and U.S. Department of Agriculture, biorefinery is defined as "A processing and conversion facility that efficiently separates its biomass raw materials into individual components and converts these components into marketplace products including biofuels, biopower, and conventional and new bioproducts." Several papers discussed the major products and integrated biorefinery concept for syngas fermentation.

Ethanol is by far the most commonly examined bioproduct that is generated during syngas fermentation. Ethanol is currently being sold as a fuel additive to blend with gasoline. The existing gasoline engines can take up to 10% ethanol (known as E10) without modifying the engine. Biomass-derived syngas fermentation also produces other important bioproducts such as acetic acid, butanol and butyric acid (Datar et al., 2004). Acetic acid has numerous applications in chemical industries including synthesis of vinyl acetate and acetic anhydride (Yoneda et al., 2001). Butanol is considered as a better transportation fuel compared to ethanol due its high energy content, and high vapor pressure. In addition, butanol is used in the production of butyl acetate and butyl acrylate which can be used as fuel additives to enhance the octane value of gasoline (Grethlein and Jain, 1992). Butyric acid is being used as a flavoring agent in the food processing industry (Zigova et al., 1999).

Apart from the main products, organic acids and alcohols, the growth of anaerobic microbes also produces valuable biochemical such as polyester which serves as an energy storage for the organism (Brown, 2006). Most of the syngas fermenting microorganisms produce these polyesters under stressed conditions such as nutrient imbalances. Polyhydroxyalkanoate (PHA) is one of the most known polyesters, produced by the cells and it is stored as a discrete granule. The polyester content of cell is as high as 80% (dry weight) (Kim and Lenz, 2001). Based on the recovery of PHA and H_2, Brown et al. (2003) proposed a biorefinery concept for syngas fermentation as illustrated in Figure 2.4.

In conventional biochemical-based ethanol plants, lignin fraction of the biomass is considered as a low-value residue. Usually, 10 to 30% of biomass feedstock contains lignin which has a higher heating value of 9,111 Btu/lb (Domalski and Milne, 1987). Therefore, the lignin recovered from the diverse feedstocks should be integrated into the process (Chakar and Ragaukas, 2004). Thermal-cracking of lignin at high temperatures ranging from 250 to 600°C showed the potential of producing low molecular weight gaseous feedstocks for further processing (Britt et al., 2000).

In an integrated biorefinery, the process is optimized to produce biofuel, along with other high-value products such as biopower, and bio-based materials for a long-term sustainability (Ragauskas et al., 2006).

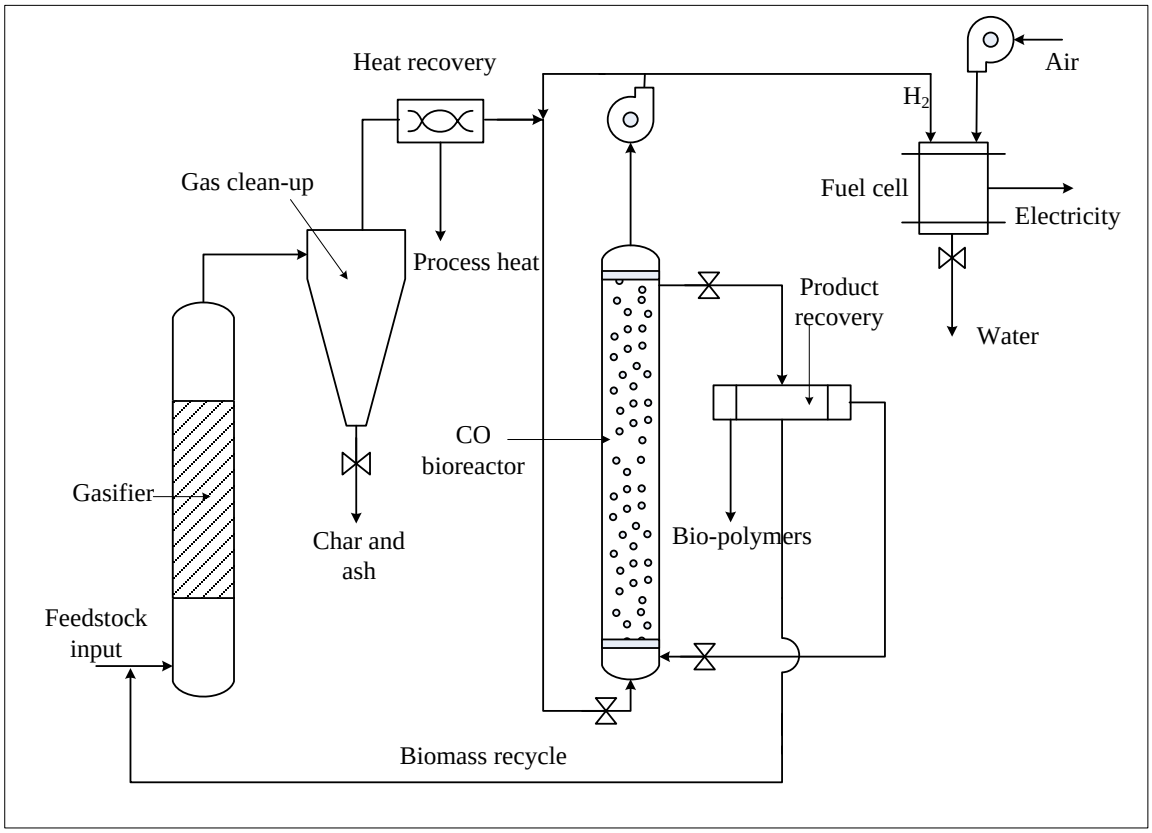

Figure 2.4. Application of biorefinery concept to produce bio-polymers and H_2 from syngas fermentation (modified from Brown et al., 2003)

2.4.2 Ethanol fermentation

Ethanol is one of the major desirable products of syngas fermentation. Ethanol is commonly used as a direct additive to gasoline. It has an octane value of 129 and the energy content is about 70% of that of gasoline (Lee et al., 2008). Most of the syngas fermenting microbes use acetyl-CoA pathway to produce ethanol (Fig.2.2). During the process, CO and H_2 are oxidized and produce electrons and H^+ ions necessary for the reactions while CO_2 gets reduced to Co-CH_3 by accepting the electrons and H^+ ions. Towards the end of the pathway, Co-CH_3 and Co-A react with CO and produces acetyl-CoA under the influence of CO dehydrogenase and acetyl-CoA synthase enzymes (Mackaluso, 2007). Acetyl-CoA acts as a building block for the production of a variety of biofuels including ethanol.

C. ljungdahlii is one of the most frequently used microorganisms in syngas fermentation to ethanol. Younesi and coworkers (2005) achieved an ethanol concentration of 0.6 g/L maintaining a syngas pressure of 1.8 atm in their bioreactor. The authors further reported that the high syngas pressure did not have a significant impact on acetic acid production, though it enhanced the ethanol yield. Klasson et al. (1990) reported a higher ethanol yield (3.0 g/L) by adding 0.02% yeast extract followed by cellobiose. The study further showed improvement in molar ratio of ethanol-to-acetate (>1.1) with the addition of 30 mg/L benzyl-viologen. Klasson et al. (1993) reported the highest ethanol concentration ever recorded (~ 48 g/L) with *C. ljungdahlii* at a pH of 4.0 - 4.5 in a completely-stirred tank reactor under limited nutrient condition during 560 h of fermentation. Maximum ethanol, acetic acid, butanol and cell yields obtained from different studies are summarized in Table 2.4.

2.4.3 Butanol fermentation

B. methylotrophicum has the ability to convert syngas into acetic acid, butyric acid, and butanol (Grethlein 1991). Shen et al. (1999) compared the physiological differences between the wild-type and the CO-adapted strains of *B. methylotrophicum,* and the production of both butyrate and butanol from CO. The authors found that the activity of the wild type *B. methylotrophicum* was completely inhibited by the presence of CO. The study further reported that the CO-adapted strain produced significant amount of butyrate while the wild type produced only trace amounts of butyrate. The CO-adapted strain produced 0.3 g/L of butanol and 0.5 g/L ethanol at pH 6.0 from the microbes grown at 100% CO.

In a different study, Worden et al. (1989) studied the possibilities of ethanol and butanol production via syngas fermentation. The authors found an increase electron flow from 6% to 70% from CO into butyrate when the pH was lowered from 6.8 to 6.0. The high level of butyrate essentially increased the butanol yield in a two-stage fermentation process (Worden et al., 1991). During the two-stage process including acidogenic and solventogenic bioconversions, Worden et al. (1991) used two different bio-catalysts, *B. methylotrophicum* and *C. acetobutylicum* in a two-stage process.

Table 2.4. Maximum product and cell yields from various studies

Microorganisms	Ethanol (g/L)	Acetate (g/L)	Cell yield (g cell/g)	Butanol (g/L)	References
C. ljungdahlii	48.0	3.0	0.4	n/a	Klasson et al., (1993)
C. ljungdahlii	3.0	2.5	n/a	n/a	Klasson et al., (1990)
C. ljungdahlii	0.1*	0.1*	1.4**	n/a	Phillips et al., (1994)
Bacterium P7(C. carboxidivorans)	0.2*	0.0*	0.3**	n/a	Rajagopalan et al., (2002)
C. ljungdahlii	0.6	1.3	0.3	n/a	Younesi et al., (2005)
C. ljungdahlii	11.5	28.0	1.2	n/a	Najafpour and Younesi, (2006)
Clostridium strain *P11(C. ragsdalei)*	25.3	4.8	1.1***	0.5	Kundiyana et al., (2010)
C. carboxidivorans	2.0	4.7	1.1***	n/a	Hurst and Lewis, (2010)
B. methylotrophicum	0.1	1.3	0.4***	0.6	Heiskanen et al., (2007)
Bacterium P7(C. carboxidivorans)	1.6	2.5	0.5***	0.5	Datar et al., (2004)
B. methylotrophicum	0.5	n/a	n/a	0.3	Shen et al., (1999)

Notes: n/a, data not available; Units, *: mol C in products per mol CO consumed;**: g/mol of CO; ***: g/L

The authors reported a high butyrate (4 g/L) and acetate (8 g/L) concentrations while the biomass recirculation was maintained. The authors further reported a butanol concentration of 2.7 g/L from the continuous operation. The eqs. (2.8) and (2.9) show the change in Gibbs free energy (ΔG°) for the reactions of CO bioconversion to butyric acid (C_3H_7COOH) and butanol (C_4H_9OH) (Worden et al.,1991).

$$10\ CO + 4\ H_2O \longrightarrow C_3H_7COOH + 6CO_2 \quad \Delta G° = -\ 40.61\ kJ/g\ mole\ CO \qquad (2.8)$$

$$12\ CO + 5\ H_2O \longrightarrow C_4H_9OH + 8CO_2 \quad \Delta G° = -\ 37.68\ kJ/g\ mole\ CO \qquad (2.9)$$

2.4.4 Methane fermentation

There are several methane-fermenting microorganisms including *Methanobacterium thermoautotrophicum, Methanothermobacter thermoautotrophicus, Methanosarcina barkeri, Methanosarcina acetivorans* strain *C2A, Rhodospirillum rubrum, and Methanobacterium formicum* (Sipma et al., 2006; O'Brien et al., 1984; Rother and Metcalf, 2004; Klasson et al., 1990) that have been isolated for bio-methane production from syngas. In syngas-to-methane fermentation, CO acts as an electron donor and CO_2 as an electron acceptor, which gets reduced to methane (CH_4). O'Brien et al. (1984) reported hydrogen production during the growth of *M. barkeri* on CO when the CO partial pressure exceeded 20 kPa. The authors further revealed a net consumption of hydrogen below CO partial pressure 20 kPa. Kluyver and Schnellen (1947) reported the production of intermediates such as H_2 and CO_2 in their suggested CO to methane pathway. Several studies reported the low growth rates of *M. barkeri* and *M. thermoautotrophicus* on CO compared to the growth on H_2 as the electron donor (Daniels et al., 1977; O'Brien et al., 1984). The possible chemical reactions and the relevant Gibbs free energy contents of the conversion of CO to methane are given by eqs. (2.10) and (2.11).

From 100% CO,

$$4\ CO + 2\ H_2O \longrightarrow CH_4 + 3\ CO_2 \quad \Delta G° = -\ 53.0\ kJ/\ mole\ CO \qquad (2.10)$$

From H_2 and CO,

$$CO + 3\,H_2 \longrightarrow CH_4 + H_2O \qquad \Delta G^\circ = -\,151.0 \text{ kJ/ mole CO} \qquad (2.11)$$

Sipma et al. (2003) reported the use of several granular anaerobic sludges to produce methane from CO at 30 and 55˚C. The authors found a significant increase in the CO to methane conversion efficiency (up to 90%). But the authors did not fully characterize the microbial communities in the sludge. According to some studies, methanogenesis is highly sensitive to CO concentration in the liquid phase (Sipma et al., 2006; Klasson et al., 1990). However, successive transfers could enhance the ability of the microorganisms to grow on 100% CO (O'Brien et al., 1984). CO fermentation to methane opens-up new area of syngas bioconversion to methane gas, which may overcome some of the challenges of syngas-to-ethanol fermentation.

2.4.5 Organic acid production

Bioconversion of syngas to organic acids (e.g., acetic and butyric acids) and alcohols (e.g., ethanol and butanol) follows the acetyl-CoA pathway (Henstra et al., 2007; Phillips et al., 1994; Klasson et al., 1990). The most common acidogenic microorganisms include *C. thermoaceticum, C. ljungdahlii, P. productus, A. woodii, Eubacterium limosum* and *B. methylotrophicum* (Grethlein and Jain, 1993). Many of the reported fermentation studies showed a high acetic acid production compared to the other organic acids. Younesi et al. (2005) reported an acetate concentration of 1.3 g/L at 1.4 atm pressure using *C. ljungdahlii*. Table 2.5 summarizes the maximum acetic acid concentrations obtained in various studies.

Butyrate is synthesized by the chemical intermediate acetyl-CoA reacting with butyryl-CoA (Brown, 2006). Acetic and butyric acid yields are highly dependent on the types of microbe and the substrate. Worden et al. (1989) reported that the production of butyrate was increased by 10-folds at the expense of acetate yield when the pH shift was from 6.8 to 6.0. Recovery of organic acids produced during syngas fermentation may provide opportunity for additional revenue generation from co-products.

2.5 Industrial-scale Syngas Fermentation

Currently, there are no industrial-scale syngas fermentation to biofuel plants. Gas-to-liquid mass transfer still considered as one of the major bottlenecks for the commercialization of syngas fermentation technology. Kundiyana et al. (2010) reported a successful operation of a 100-L pilot-scale syngas fermentation facility. Regardless of the recent developments in reactor designs, process optimizations, and microbial catalysts selection, the ethanol concentration from syngas fermentation is still just under 30 g/L (Gaddy et al., 2007). This leads to a high cost of ethanol recovery. For cost effective ethanol recovery, its concentration should be around 15% (*v/v*). Therefore, in order to reduce the recovery cost, thus improving the overall economy of the process, industrial-scale syngas fermentation should focus on achieving higher ethanol concentration. This requires significant research and development in process microbiology.

Currently, there are three major companies developing syngas fermentation technology; namely, IneosBio, Coskata and LanzaTech. All these companies indicated successful operation of larger facilities with higher ethanol yields (Kopke et al., 2011). In 2011, Coskata announced two years of successful operation of their 'semi-commercial' syngas fermentation facility in Madison, PA, USA (Coskata press release: http://www.coskata.com/company/media.asp?story=504B571C-0916-474E-BFFA-ACB326EFDB68). However, with falling natural gas price, Coskata has shifted its priority from biomass feedstocks to natural gas for syngas production.

2.6 Key Performance Index

Biomass pre-treatment, feedstock properties, gasification method, gas clean-up and conditioning and fuel synthesis are among the key performance parameters involve in syngas fermentation (McKendry, 2002). Biomass pre-treatment can be further subcategorized into unit processes such as drying, size reduction, fractionation and leaching. In general, before gasification the moisture content of the biomass should be below 15% and the typical feed particle size is around 20-80 mm. Fractionation and leaching with water reduce the nitrogen and alkali content of the feedstock producing lesser impurities in the gas mixture.

Characteristics of the biomass feedstocks such as moisture content, ash content and volatile compounds have a significant impact on syngas fermentation. Biomass with moisture contents above 30% make the gasification difficult and reduce the calorific value of the produced gas (McKendry, 2002). Higher mineral content of the biomass leads to a higher ash production during gasification. Clinkering or slagging problems in the pipe lines are common in biomass with higher ash contents. Production of tar and other volatile substances during gasification leads to cell dormancy and process inhibitions in syngas fermentation (Ahmed and Lewis, 2007).

Gasification technology is a key operational parameter in syngas fermentation. In general, there are two major types of gasifiers namely, fixed bed and fluidized bed gasifiers. Fixed bed gasifiers are further classified as updraft, downdraft or cross-flow depending on the airflow direction. Generally, fixed bed gasifiers produce lesser amount of particulate matter than fluidized bed gasifiers, where as the calorific value of the produced gases in the fixed bed gasifier is lower than that of the fluidized bed gasifiers. However, fixed bed gasifiers are relatively simple in design compared to the complex design of the fluidized bed.

Gas clean-up and conditioning remove the problematic tars, chars, particulate matters and other contaminant compounds which cause pipe slaggings and downstream process inhibitions. Cyclones, adsorption columns, water or oil scrubbers and various types of filters are some of the common syngas purification unit operations.

Fuel synthesis and the product recovery are the key parameters that describe the efficiency and the economic feasibility of the fermentation process. Further, the efficiency of the process can be increased by adapting innovative reactor designs with higher mass transfer rates, new biocatalysts with increased product yields and efficient product recovery methods such as membrane separation and nano particles.

CHAPTER 3

MATERIALS AND METHODOLOGY

3.1 Experimental Set-up

A schematic diagram of a typical experimental set-up is shown in Figure 3.1 (see Appendix A for pictures of reactor configurations). The experiments were conducted using tap water at 25±2˚C as the aqueous medium with pH of 7.6±0.2. The working volume for all reactor configurations was maintained at 3.0 L. During each experimental run, compressed bottled carbon monoxide (CO) gas (Airgas, Gaspro, Honolulu, HI) with purity of 99.99% was sparged into water through different diffusers in the reactors. The CO flow rate was measured by a 150-mm rotameter (Omega, FL-3000, Stamford, CT) specially calibrated for CO gas. Water recirculation was carried out using a digital peristaltic pump (Masterflex L/S 7523-60, Vernon Hills, IL) and maintained a constant recirculation flow rate of 0.5 L/min. Tygon hard tubing (10 mm diameter) was used to connect the recirculation ports and the liquid samples were withdrawn through a three way sampling port with a septa located 120 mm away from the reactor outlet, using 10 µL gastight high performance syringes (Hamilton Gastight1701, Reno, NV). Initial liquid sample was withdrawn before introducing the CO into the reactor and the subsequent samples were collected at an interval of 15 s in each reactor configuration. It was assumed that there was a homogeneous mixing within the aqueous phase in the reactor.

All the experiments, except the composite hollow fiber (CHF) membrane module, were conducted under a pressurized (up to 10 psig) CO flow. The experiments were repeated for CO flow rates ranging from 2 to 5 L/min. The submerged CHF membrane module was operated under three different CO pressures: 25, 30, and 35 psig. Table 3.1 summarizes the operational conditions and diffuser types in various reactor configurations used in this study.

3.2 Reactor Configurations

3.2.1 Column diffuser

The reactor was equipped with a column diffuser (Fig. 3.1) (Alita Industries Inc., ST-100, Arcadia, CA) which was used to sparge CO into the liquid phase. The pore size of the silicon membrane on the outer surface of the diffuser was between 0.5 to 1 mm and the height and the diameter were 150 mm and 25 mm, respectively. The experiment was carried out for CO flow rates of 2, 3, 4, and 5 L/min. The liquid samples were extracted through a septa located at 120 mm away from the outlet port (see Appendix A for various types of diffusers).

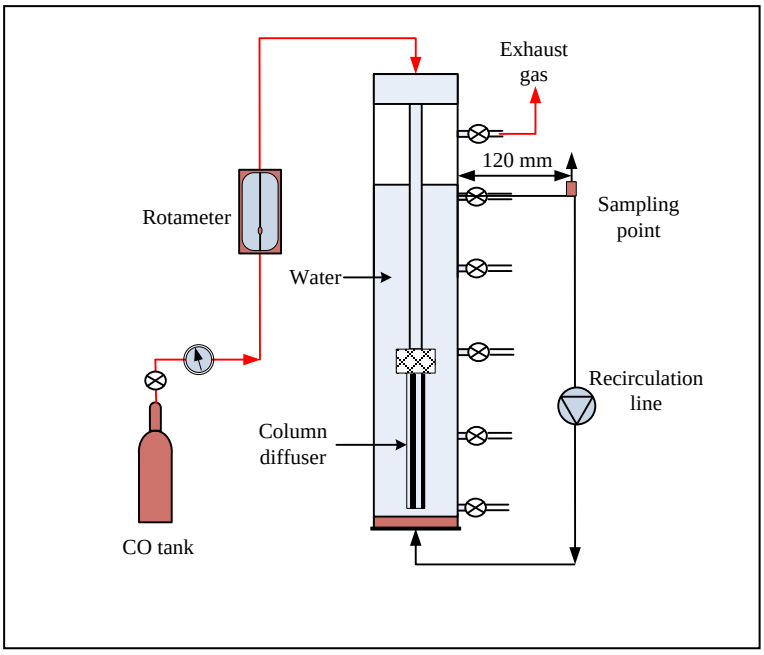

Figure 3.1. Experimental set-up for mass transfer studies using a column diffuser

3.2.2 20-μm bulb diffuser

In this configuration, CO gas was introduced into the reactor through a 20-μm bulb diffuser (pore size 20-μm) (Alita Industries Inc., Arcadia, CA). The experimental set-up of the reactor was similar to the column diffuser reactor, except the use of 20-μm bulb diffuser instead of the column diffuser.

Table 3.1. Operational conditions for different reactor configurations

Reactor types	Operational conditions			Manufacturers
	Description	CO pressure (psig)	CO flow rate (L/min)	
Column diffuser	150 mm long and 25 mm diameter column diffuser with pore diameters from 0.5 to 1.0 mm	10	2, 3, 4, and 5	Alita Industries Inc.
20-µm bulb diffuser	Pore diameter 20-µm	10	2, 3, 4, and 5	Alita Industries Inc.
Sparger only	Ring sparger (ring diameter 50 mm) with 0.5 mm diameter pores	10	2, 3, 4, and 5	n/a*
Sparger with mechanical mixing	Ring sparger with 450 mm impeller for two different mixing speeds (150 and 300 rpm)	10	2, 3, 4, and 5	Fisher Scientific
Submerged composite hollow fiber (CHF) membrane module (hydrophobic type)	CHF membrane (MHF 0504 MBFT) was submerged in water and purged the high pressurized CO gas through the fibers from inside to outside. The membrane had a surface area of 0.6 m^2	25, 30, and 35	n/a*	Mitsubishi Rayon Co.
Air-lift combined with a 20-µm bulb diffuser	20-µm bulb diffuser with a daft tube (55 mm diameter and 330 mm height)	10	2, 3, 4, and 5	n/a*
Air-lift reactor combined with a single point gas entry	Single point gas entry (3 mm diameter), draft tube (55 mm diameter and 330 mm height)	10	2, 3, 4, and 5	n/a*

* Not applicable

3.2.3 Sparger only

A 2-inch diameter ring with 0.5 mm diameter pores was used to sparge CO into the aqueous phase. The ring was placed at the bottom of the reactor facilitating better mixing and higher gas retention time.

3.2.4 Sparger with mechanical mixing

This configuration was a combination of the ring sparger and a mechanical mixing device. The mechanical mixing device comprised of two radial-flow (Rushton-type) and axial flow impellers. Similar to the previous configuration the CO gas was sparged from the bottom and the impeller was inserted from the top of the reactor. The experiment was repeated for two impeller rotational speeds: 150 and 300 rpm. Vortex formation was controlled by placing equally spaced baffles along the wall.

3.2.5 Submerged composite hollow fiber (CHF) membrane system

A composite hollow fiber membrane module (MHF 0504 MBFT, Mitsubishi Rayon Co., NY) was operated under submerged condition for three different CO gas pressures: 25, 30 and 35 psig. The pressurized CO was introduced into the aqueous phase through membrane fibers. The liquid samples were extracted in 30 s intervals and the experiments were performed in triplicates to minimize the experimental error. The surface area of the membrane module was 0.6 m^2 and the module length was 200 mm. According to manufacturer's specifications, the membrane was reported to withstand a maximum pressure of 43 psig.

3.2.6 Air-lift combined with a 20-μm bulb diffuser

In this reactor configuration, the air-lift reactor was combined with a 20-μm bulb diffuser to enhance the mass transfer. The draft tube diameter and the height of the reactor were 55 mm and 330 mm, respectively. A 50-mm gap was maintained between the draft tube and the bottom of the reactor to facilitate high liquid flow-rate.

3.2.7 Air-lift combined with single point gas entry

Instead of a 20-μm bulb diffuser, this system consisted of a single gas entry point (3 mm diameter) located at the center of the bottom of the reactor.

3.3 Determination of Dissolved CO Concentration

3.3.1 Myoglobin (Mb)-protein method

Carbon monoxide concentration of the samples was measured by myoglobin (Mb)-protein bioassay. The detailed procedure can be found elsewhere (Kundu et al., 2003), but a brief summary is included in the following paragraphs.

Myoglobin (Mb)-protein was obtained from a horse heart as a lyophilized powder (Sigma-Aldrich, Saint Louis, MO) with a purity of > 90%. Liquid samples with unknown CO concentrations were prepared in a 1.5 mL-semi-micro polystyrene disposable cuvettes (Fisher scientific, Pittsburgh, PA) by adding 1 mL of 0.1 M potassium phosphate buffer solution at pH 7.0. Small amount of sodium dithionite ($Na_2S_2O_4$) was then added into the cuvette to scavenge the dissolved oxygen (DO) in the solution. The myoglobin solution was prepared by dissolving a weighted amount of Mb in a known volume of 0.1 M potassium phosphate buffer. The volume of Mb added into each sample was determined by the maximum peak (absorption value around 1.7) for the CO saturated sample and the Mb solution concentration. Finally, 10 µL of CO free, CO saturated or the unknown CO concentration sample was added and scanned in the wavelength range of 400 to 700 nm. The highest absorption peak for carboxymyoglobin (MbCO) occurred at a wavelength of 423 nm. The data file generated in the spectrophotometer (DR 5000, HACH, Loveland, CO) was then saved in an external storage device and uploaded to a software called SpectraSolve (Ames Photonics, Hurst, TX) as a text file for further analysis. During the analysis, the resulting spectra from unknown samples were fitted between the CO-saturated and CO-free absorption profiles. The percentage similarity of each profile with the CO-saturated base line was obtained by the SpectraSolve software. Actual CO concentrations of the samples were then determined using the following equation.

$$\text{CO concentration in aqueous phase} = (C_p)(SS)(V_t/V_s) \qquad (3.1)$$

Where, C_p is the protein concentration (µM), SS is the percentage of CO saturated spectra obtained from SpectraSolve (%), V_t is the total volume of the sample in the cuvette (µL), and V_s is the sample volume in the cuvette (µL). The protein concentration was determined using the Beer-Lambert law.

(3.2)

$$C_p = A/l.\varepsilon_a$$

Where, A is the absorption value, l is the cell path length (cm), and ε_a is the molar absorptivity (for Mb, ε_a =188 1/μM.cm).

3.3.2 Gas chromatograph equipped with thermal conductivity detector (GC-TCD) method

The head space CO gas samples were analyzed by gas chromatography method. The gaseous phase CO concentration data was then transferred to the aqueous phase using Henry's law (eq. (3.3)). The dissolved CO concentrations were then used to determine the gas-liquid mass transfer rates over a range of volumetric gas flow rates (1 ≤ Q ≤ 5 L/min).

$$H = \frac{P_A}{x} \qquad (3.3)$$

Where, H is the Henry's law constant (atm), P_A is the partial pressure of gas above the aqueous phase (atm) and x is the mole fraction of gas in the solution (unitless) (Smith and Harvey, 2007). Henry's law constants used for H_2 and CO in this analysis were 7.09 x10^4 and 5.82 x10^4 atm (at 25˚C and 1 atm), respectively (Wilhelm et al., 1977).

3.3.3 Determination of k_La for H_2 and CO

Assuming that the concentration in the liquid phase at the gas-liquid interface is in equilibrium with the gas concentration in the gaseous phase, the volumetric mass transfer co-efficient (k_La) in the absence of any microorganisms was determined using the following equation:

$$\frac{dC}{dt} = k_L a(C_i - C) \qquad (3.4)$$

Where, C is the gas concentration in the liquid phase (mg/L) at any giver (s) and C_i is the saturated gas concentration (mg/L). Eq. (3.4) can be further simplified to (eq. (3.5)),

$$ln\left(\frac{C_i - C_0}{C_i - C}\right) = (k_L a)t \qquad (3.5)$$

Where, C_0 is the initial gas concentration in the liquid phase (mg/L).

3.3.4 Determination of overall volumetric mass transfer coefficient (Ka) in mixed syngas experiment

Mixed syngas experiment was carried out using CHF membrane bioreactor. A customized syngas composition of 20% CO, 10% H_2, 15% CO_2, and 55% N_2 was used in the analysis. The CO and H_2 concentrations in the liquid phase were determined using Mb-protein bioassay and GC-TCD methods, respectively.

3.4 Determination of Dissolved H_2 Concentration

H_2 gas samples were collected from a three-way gas sampling port at an interval of 25 s for 2.5 minutes. The first gas sample was collected at 8 s after the introduction of H_2 gas into the reactor. The gas compositions were then determined using GC (Perkin Elmer, Auto system, Waltham, MA) with a 40/60 mesh carboxen 1000 column (Supelco Inc., Bellefonte, PA) connected to a thermal conductivity detector (TCD) with helium (He) as the carrier gas. The carrier gas flow rate was maintained at 20 mL/min. The TCD was operated at 35˚C for 5 min, after which the temperature was ramped up to 225˚C at a rate of 20˚C/min. The head space gas concentration was then converted to the aqueous phase concentration using Henry's law (eq. (3.3)).

3.5 Microbial Culture Media

Clostridium carboxidivorans (P7) (ATCC, BAA 624) was utilized in the syngas fermentation experiments. The bacterium was grown under strict anaerobic conditions in a medium containing 30 mL of mineral stock solution, 10 mL of trace metal solution, 10 mL of vitamin stock solution, 0.5 g yeast extract, 5 g of morpholinoethanesulfonic acid (MES), and 10 mL of 4% cystein-sulfide solution. Resazurin solution (0.1%) was added as the redox indicator. The composition of the minerals, trace metals and the vitamin stock solutions were previously described (Datar et al., 2004). The batch fermentation experiments were carried out in 250 mL serum bottles with a liquid media volume of 110 mL. Gas and liquid samples were obtained from each fermentation bottle to determine the CO concentration in both gas and liquid phases. Fermentation was carried out in three different syngas compositions as given in Table 3.2.

Table 3.2. Gas compositions used in the fermentation experiment with *C. carboxidivorans* culture media

Conditions	CO (%)	CO_2 (%)	H_2 (%)	N_2 (%)
1	40	15	10	35
2	20	15	10	55
3	10	15	10	65

3.6 Model Analysis

3.6.1 Composite hollow fiber (CHF) membrane reactor configuration

A schematic diagram of the CHF membrane (MHF0504MBFT, Mitsubishi Rayon Co, NY) reactor used in the mass transfer analysis and modeling is shown in Figure 3.2. The membrane module was operated in dead-end operational mode and the pressurized gas (CO, H_2 or syngas) was introduced into the shell side of the membrane (outside-in mode). The liquid was recirculated through the membrane fibers and the gas saturated liquid was pumped back to the main reactor by using a recirculation pump. Liquid samples were collected from the sampling line through a three-way septum. The main properties and the operations parameters of the membrane modules used in the analysis (model development and testing) are given in Table 3.3. In this case, separate models were developed for CO and H_2 gases by using the model equations developed as described in section 3.6.2.

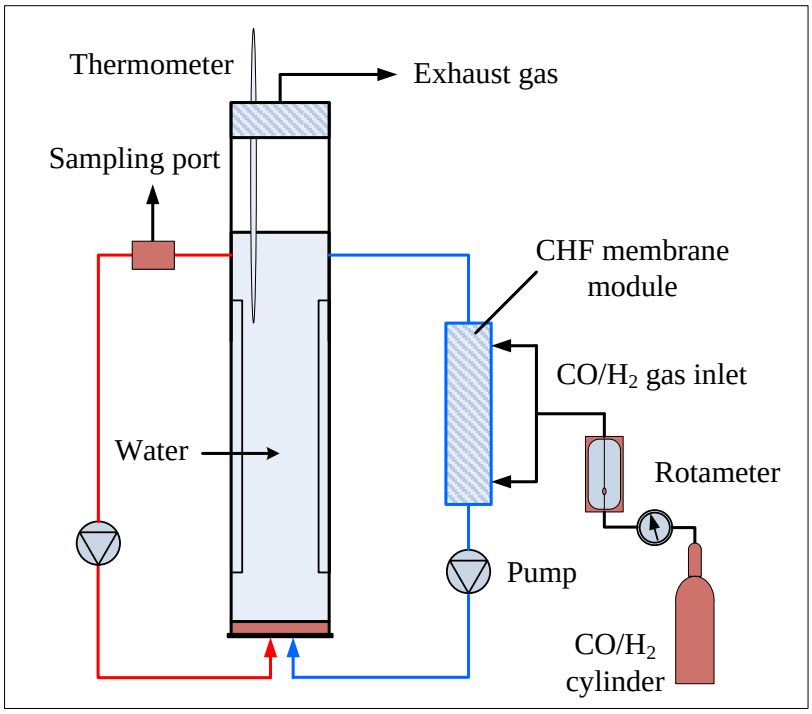

Figure 3.2. Composite hollow fiber (CHF) membrane bioreactor

Table 3.3. Properties and the operational parameters of the membranes used in model development and testing

Parameters \ Membrane types	PDMSXA-2500	MHF0504 MBFT	PDMSXA-8300
Length of the module (mm)	140	200	140
Maximum external diameter (mm)	32	48	51
Membrane surface area (m^2)	0.25	0.60	0.83
Fiber internal diameter (µm)	200	200	200
Wall thickness of the membrane (µm)	50	40	50
Material of housing and cap	Polycarbonate	Polycarbonate	Polycarbonate
Maximum operating pressure (psig)	< 45	< 45	< 45
Operating temperature (°C)	0 to 90	0 to 40	0 to 90
Sealant	Polyurethane	Polyurethane	Polyurethane

3.6.2 Model development

The gas (CO or H_2) transfer characteristics of the CHF membrane were evaluated by monitoring the rate of change of dissolved gas concentrations with time in the main reactor which was connected with the CHF membrane module through a recirculation line. The reactor concentration versus time data was analyzed by using the model equation developed as follows.

From Henry's law,

$$P_A = HC^* \tag{3.6}$$

Where, P_A is the partial pressure of a component gas (atm), C^* is the aqueous phase gas concentration (mg/L) and H is the Henry's law constant (atm.L/mg).

For steady state operation gas flux across the membrane F (mg/s.cm^2),

$$F = K(C^* - C_L) \tag{3.7}$$

Where, K is the overall mass transfer coefficient (cm/s) and C_L is the gas concentration in the aqueous phase (mg/L).

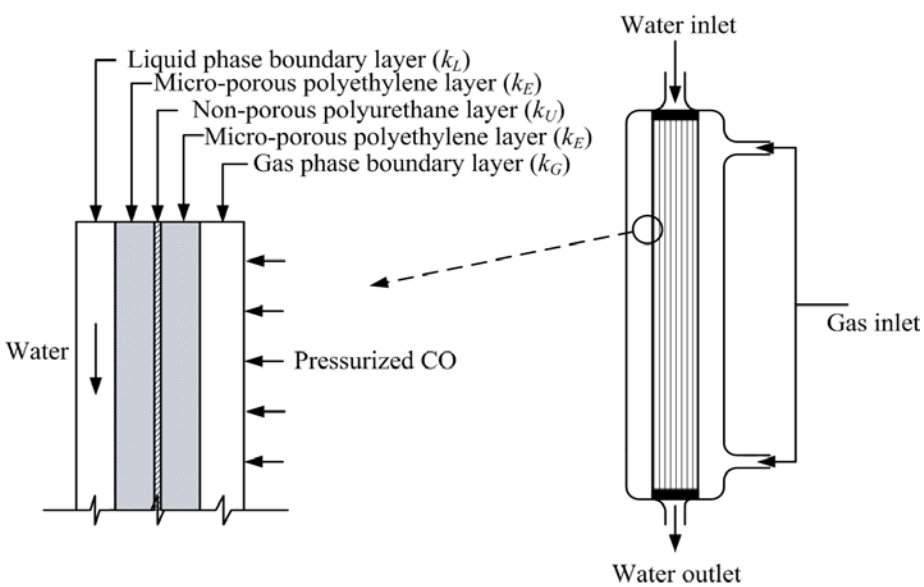

Figure 3.3. Flow directions and mass transfer across the membrane fibers

The overall mass transfer resistance can be written as a summation of the individual mass transfer resistances. In a CHF membrane, the mass transfer between gas and liquid phases involves five different transport resistances (Fig. 3.3); (1) the feed gas boundary layer (k_G); (2) the microporous polyethylene layer (k_E); (3) the non-porous polyurethane layer (k_U); (4) the micro-porous polyethylene layer (k_E); and (5) the liquid boundary layer (k_L). Therefore, the overall mass transfer coefficient (K) or resistance to mass transfer through the membrane ($1/K$) is given by eq. (3.8);

$$\frac{1}{K} = \frac{1}{k_L} + \frac{1}{Hk_E} + \frac{1}{Hk_U} + \frac{1}{Hk_E} + \frac{1}{Hk_G} \tag{3.8}$$

Typically, in membrane resistance analysis, one of the individual resistant coefficients is smaller than the others, thus contributing significantly to the mass transfer resistance ($1/K$). The resistances offered by the gas-filled porous polyethylene layers ($1/Hk_E$) of the CHF membrane and the gas phase boundary layer resistant ($1/Hk_G$) are negligible (Voss et al., 1999). Therefore, the overall membrane resistance equation can be given by eq. (3.9);

$$\frac{1}{K} = \frac{1}{k_L} + \frac{1}{Hk_U} \tag{3.9}$$

In this case membrane resistance ($1/Hk_U$) can be determined by plotting the reciprocal of observed mass transfer coefficient ($1/K$) and the reciprocal of the water velocity ($1/v_L$) (Ahmed et al., 2004). Once the membrane resistance ($1/Hk_U$) is known, the liquid boundary layer resistance coefficient ($1/k_L$) can be calculated for each K value by using eq. (3.9).

CO mass transfer across a single fiber can be written as,

$$v_L \frac{dC_L}{dz} = Ka(C^* - C_L\ ) \tag{3.10}$$

Where, v_L is the liquid velocity (cm/s) through the membrane and a is the surface area to volume ratio of the membrane (1/cm) (specific surface area of the membrane).

Using the boundary conditions and after integration,

$$C_2 = C^* - (C^* - C_1)\exp\left(-Ka\frac{L}{v_L}\right) \tag{3.11}$$

Using mass balance,

$$V\frac{dC_1}{dt} = Q(C_2 - C_1) \tag{3.12}$$

Combining eqs. (3.11) and (3.12),

$$\frac{dC_1}{C^* - C_1} = \frac{Q}{V}\left[1 - exp\left(-Ka\frac{L}{v_L}\right)\right]dt \tag{3.13}$$

Integrating with the boundary conditions when $t=0$, $C_1=0$ and $t=t$, $C_1=C_1$,

$$\ln\left(\frac{C^*}{C^* - C_1}\right) = \frac{Q}{V}\left[1 - exp\left(-Ka\frac{L}{v_L}\right)\right]t \tag{3.14}$$

In order to normalize the data, the obtained mass transfer data for each pressure and recirculation flow rate are presented in non-dimensional form using Reynolds number (*Re*), Sherwood number (*Sh*) and Schmidt number (*Sc*) as define follows (eqs. (3.15)-(3.17)),

$$Sh = \frac{Kd}{D} \tag{3.15}$$

$$Re = \frac{v_L d}{\nu} \tag{3.16}$$

$$Sc = \frac{\nu}{D} \tag{3.17}$$

Where, ν is the kinematic viscosity of water (cm^2/s), D is the molecular diffusivity of CO in water (cm^2/s) and d is the internal diameter of the membrane fibers (cm). In this case, Sherwood number (*Sh*) is considered as the ratio of molecular mass transport resistance to the convective mass transfer resistance of the fluid. Further, the Reynolds number (*Re*) is defined as the ratio between the inertial forces and the viscous forces. The Schmidt number (*Sc*) is defined as the ratio between the momentum diffusivity and mass diffusivity.

3.7 Model Testing

The testing of the models was carried out by using several other membrane modules (polydimethyl siloxane) (PDMSXA-2500 and PDMSXA-8300, Medarray Inc., Ann Arbor, MI). The main properties of the membrane modules are shown in Table 3.3. The membrane bioreactor experiments were conducted under dead-end outside-in operational mode and a description various operational conditions are shown in Table 3.4. Further, the experiments were repeated for both H_2 and CO gases and each runs were conducted in triplicates.

3.8 Statistical Analysis

The statistical analysis software (SAS) was used in order to rank the reactor configurations according to their significance in terms of their mass transfer efficacy. For the analysis, CO flow rate and the reactor configurations were uploaded into the software model as independent variables, while CO concentration was selected as the dependant variable. Duncan's multiple range test and Bonferroni (Dunn) t tests were carried out to group the reactors according to their significance.

Further, In the case of model development and testing, a Duncan's multiple range and Bonferroni t-tests were carried out to determine the significance of CO inlet pressure and recirculation flow rates. The α value was selected as 0.05 for all statistical analysis models.

Table 3.4. Membrane types and other operational conditions for testing of the mass transfer model

Membrane types	Operational conditions	
	Gas inlet pressure (psig)	Recirculation flow rate (mL/min)
PDMSXA-2500	10	400, 800, and 1600
	15	
	20	
PDMSXA-8300	10	400, 800, and 1600
	20	
	40	

CHAPTER 4

RESULTS AND DISCUSSION

4.1 Developing a Correlation between Myoglobin (Mb)-Protein and Gas Chromatograph Equipped with Thermal Conductivity Detector (GC-TCD) Methods

4.1.1 Carbon monoxide mass transfer

Carbon monoxide –water mass transfer data was obtained using myoglobin (Mb)-protein bioassay and the gas chromatograph equipped with thermal conductivity detector (GC-TCD) method. The variation of $ln\ [(C_i-C_0)/(C_i-C)]$ with time acquired from these two methods are shown in Figures 4.1 and 4.2. The highest volumetric mass transfer coeffcient (k_La) values of 117.7±3.6 and 100.0±2.8 1/h for CO were obtained from the GC-TCD method and the Mb-protein bioassay, respectively. Riggs and heidel (2006) reported a k_La value of 76 1/h for CO using a stirred tank reactor with an agitational speed of 400 rpm. However, increasing agitational speeds would not consider to be an economical approach in order to obtain higher mass transfer rates.

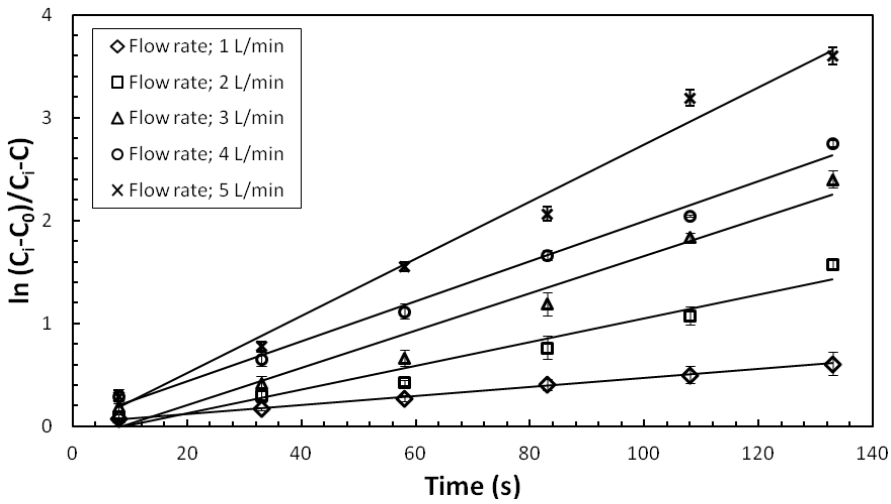

Figure 4.1. Variation of $ln\ [(C_i-C_0)/(C_i-C)]$ with time (Mb-protein method) for different CO flow rates

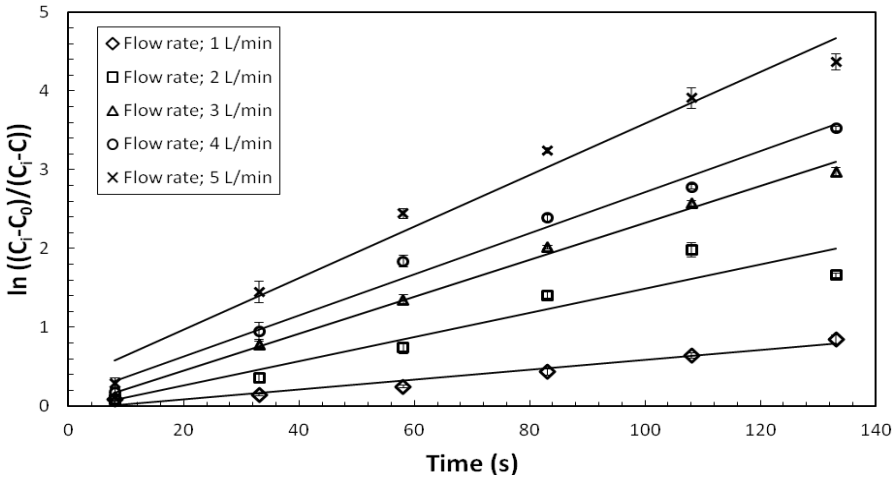

Figure 4.2. Variation of *ln* $[(C_i-C_0)/(C_i-C)]$ with time (GC-TCD method) for different CO flow rates

The presence of gas bubbles in the extracted sample was the most common experimental error associated with Mb-protein bioassay. Under these conditions, extracted samples showed a higher CO concentration caused by continuous CO diffusion from the bubbles. This was a critical factor, especially at higher CO flow rates, which resulted in higher variations in aqueous phase CO concentration. Analyzing triplicate samples and multiple trials were able to minimize the experimental errors.

4.1.2 Correlation between k_La values for CO obtained from Mb-protein bioassay and GC-TCD method (without culture media)

All previous studies on syngas fermentation evaluated the fermentation efficacy based on dissolved CO concentrations determined using GC analyses and Henry's law. It is therefore, critically important to develop a correlation between the Mb-protein bioassay method and the GC analysis method for determining dissolved CO in the aqueous phase. The correlation between the two methods of determining k_La for CO in the aqueous phase for various flow rates is shown in Figure 4.3. The correlation factor (R^2) for the variation was 0.98. Further, the gradient of the graph, i.e. the ratio between the k_La values obtained from the Mb-protein bioassay and the GC-TCD method was around 79%. This means that the k_La values obtain from Mb-protein bioassay were significantly close to the values

acquired using GC-TCD method. Thus, the Mb-protein bioassay, which is much simpler, quicker and cheaper method than the GC-TCD method can be reliably used to determine the CO concentration in the aqueous phase.

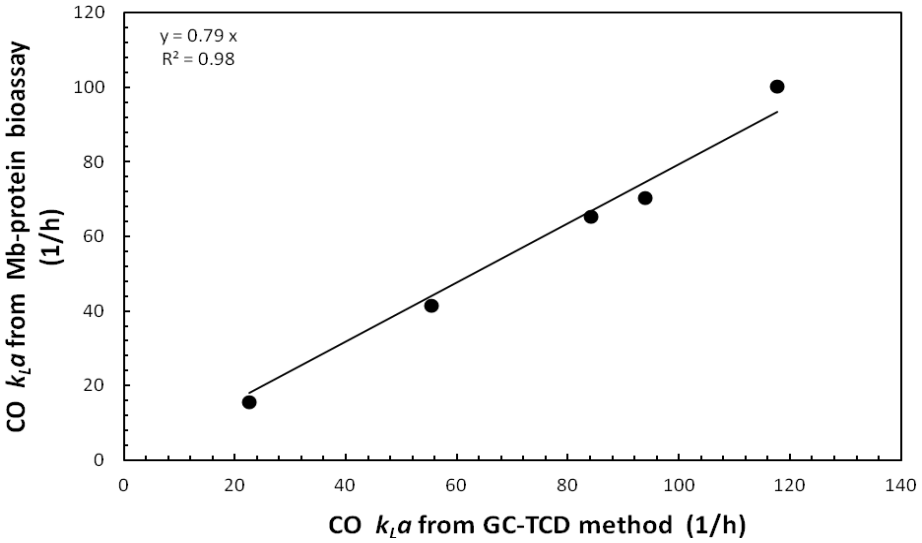

Figure 4.3. Correlation between the CO k_La values obtained from Mb-protein and GC-TCD methods (without culture media)

4.1.3 Correlation between k_La values for CO obtained from Mb-protein bioassay and GC-TCD method (with C. carboxidivorans media)

C. carboxidivorans was used as the microbial culture to develop a correlation between Mb-protein and GC-TCD methods to obtain CO in the aqueous phase. The experiment was carried out in 250-mL serum bottles under different syngas compositions. Liquid and gas samples were obtained simultaneously from each serum bottle for the correlation analysis. Figure 4.4 shows the variation of the CO concentration obtained from the Mb-protein bioassay and the GC-TCD method. Interestingly, a similar correlation (R^2=0.99) was observed with *C. carboxidivorans* culture media (see Appendix C for standard curve details).

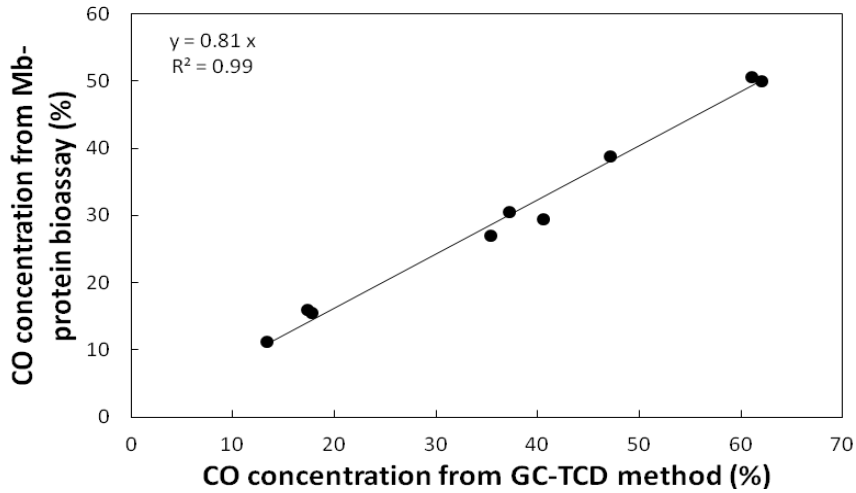

Figure 4.4. Correlation between k_La values obtained from Mb-protein and GC-TCD methods (with *C. carboxidivorans* culture media) for CO

This means that the k_La values obtained from Mb-protein bioassay were close to the values acquired using GC-TCD method. Further, this validates the use of Mb-protein bioassay to determine the dissolved CO concentrations in both with and without culture media. Moreover, the Mb-protein bioassay and the correlation developed in this study, is extremely important for a vast majority of the research community who needs a much simpler, quicker and cheaper method than the GC-TCD method to determine the CO concentration in the aqueous phase.

4.2 Determination of Volumetric Mass Transfer Coefficients (k_La) of CO Using Different Reactor Configurations

4.2.1. Mass transfer

Mass transfer data were acquired for CO dissolved in water for different reactor configurations and flow rates of $2 \leq Q \leq 5$ L/min. In composite hollow fiber (CHF) membrane module, the experiment was conducted under three different CO pressures of 25, 30, and 35 psig. Figure 4.5 shows a typical CO concentration profile as a function of time for different CO flow rates. As expected, the CO concentration in the liquid phase

increased with CO flow rate and the sparging time. Three trials for each operating condition were conducted and an average volumetric mass transfer rate was calculated to minimize potential experimental errors. The theoretical CO saturation concentration in an aqueous phase under room temperature and atmospheric pressure was reported around 26.6 mg/L (Bredwell and Worden, 1998). However, the maximum CO concentration achieved for all reactor configurations in this study was between 23 and 25 mg/L. The slightly lower value obtained in this study could be due to CO sparging time that was short to reach the saturation level especially at low CO flow rates. Gas bubbles in the extracted sample syringes was the most common experimental error associated with myoglobin-protein method. Under these conditions, extracted samples showed higher CO concentration caused by continuous CO diffusion from the bubbles. This phenomenon was mainly observed during higher CO flow rates.

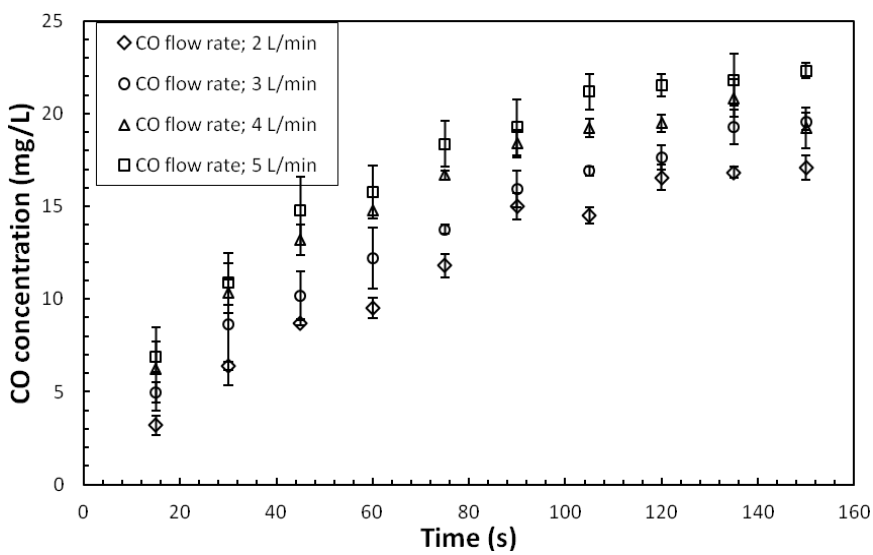

Figure 4.5. Typical CO concentration profile for different flow rates

Once the CO concentration in the liquid phase was determined, the k_La values for each condition were calculated by fitting the data into eq. (3.5). In this case the initial CO concentration in the sample was assumed to be zero (Riggs and Heidel, 2006). Theoretically, the relationship between $ln\ [(C_i\text{-}C_0)/(C_i\text{-}C)]$ and (k_La) t is linear and the gradient of the straight line gives the k_La value. Figure 4.6 shows the k_La values derived

for the conditions shown in Figure 4.5. The correlation factor (R^2) for the plots was in the range of 0.97 to 0.98. At lower CO flow rates, R^2 was close to 1.0 since there were no gas bubbles in the extracted samples. The highest k_La value was obtained at the highest CO flow rate of 5 L/min.

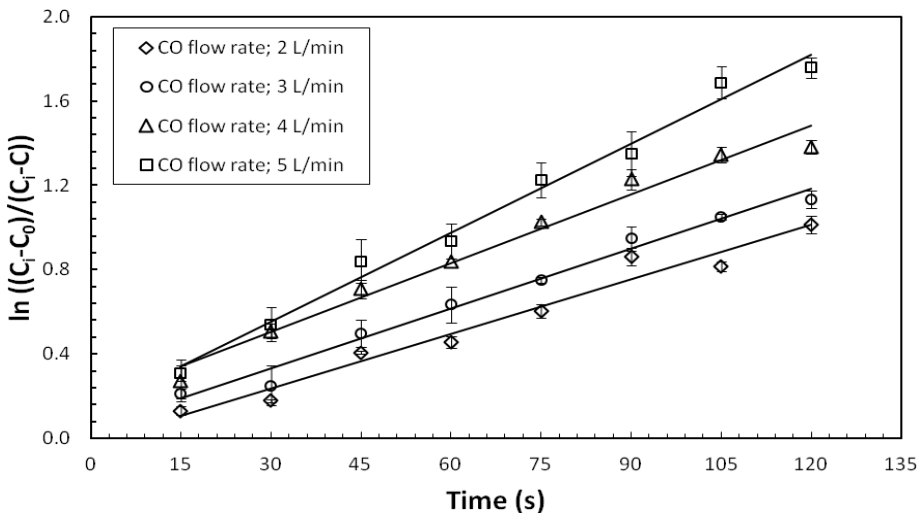

Figure 4.6. Variation of *ln [(Ci-C0)/(Ci-C)]* with time for different CO flow rates

Figure 4.7 shows the variation of k_La as a function of CO flow rate for different reactor configurations except for the CHF membrane reactor. The k_La values reported in this study (Figure 4.7) ranged from 2.5±0.1 to 91.1±5.3 1/h. The highest volumetric mass transfer coefficient was obtained in the air-lift reactor combined with a 20-μm bulb diffuser (91.1±5.3 1/h) while the reactor with the column diffuser has the lowest k_La value (2.5±0.1 1/h). However, Brewell et al. (1999) reported k_La values raging from 104 to 190 1/h using a stirred-tank reactor combined with microbubble sparger. The reactors having only a 20-μm bulb diffuser and air-lift combined with a single gas entry point showed lower k_La values than the air-lift reactor combined with a 20-μm bulb diffuser. Further, a slight increase in mass transfer was observed in the sparger combined with mechanical mixing reactors when the mixing speed was increased from 150 rpm to 300 rpm. On the other hand, reactors having larger pore sizes such as column diffuser and sparger only, showed a limited CO solubility in the aqueous phase, highlighting the poor

efficacy of mass transfer due to larger pore sizes. This suggests that the pore size of the diffuser is critically important for mass transfer and could be enhanced further by introducing a slight agitation in the reactor. Further, the air-lift configuration has a higher gas retention time compared to the other reactors resulting higher CO diffusion into the liquid phase (see Appendix B for other $ln\ [(C_i-C_0)/(C_i-C)]$ data).

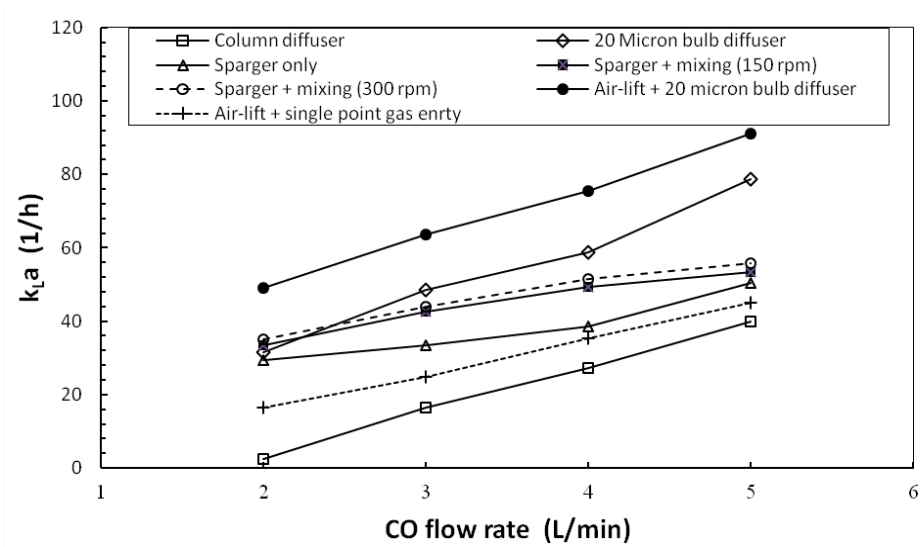

Figure 4.7. Volumetric mass transfer coefficient (k_La) as a function of CO flow rate for various reactor configurations

The k_La values reported in many studies (Table 2.3) are lower than this study. This is mainly because the current study was conducted in the absence of microorganisms. Thus, it does not include additional mass transfer resistance of gaseous substrate to the surface of the microorganisms. Riggs and Heindel (2006) obtained higher k_La values (ranging from 10.8 to 155.01/h) in their stirred-tank experiment. The study was, however conducted at higher agitation speeds (up to 600 rpm) and higher CO flow rates (up to 6 L/min).

4.2.2 Submerged composite hollow fiber (CHF) membrane reactor

The determination of volumetric mass transfer coefficient for the submerged CHF membrane was slightly different from the rest of the reactor configurations. As mentioned earlier, submerged CHF membrane was operated under dead-end, inside-out

mode and the experiment was repeated for three different pressures: 25, 30, and 35 psig. Figure 4.8 shows the CO concentration as a function of time for three different pressure values. Under these conditions, the highest CO concentration was found to be 2.5 mg/L after seven minutes of operation.

Based on CO concentrations, the volumetric mass transfer coefficients were then determined. The maximum $k_L a$ obtained for the CHF membrane reactor was 1.1 1/h. The main reason for the low mass transfer is the smaller driving force (i.e., CO concentration difference between inside the membrane fiber lumen and the thin liquid layer (boundary layer) attached to the surface of the membrane fiber). At the beginning of the experiment the CO concentration inside the fiber lumen was higher than that of the boundary layer (membrane resistance). Over time, the gas diffused into the thin boundary layer (resistance due to the membrane and the boundary layer). Since the boundary layer is a thin liquid film, it saturates with CO quickly and the CO concentration gradient drops down leading to a lower mass transfer rate.

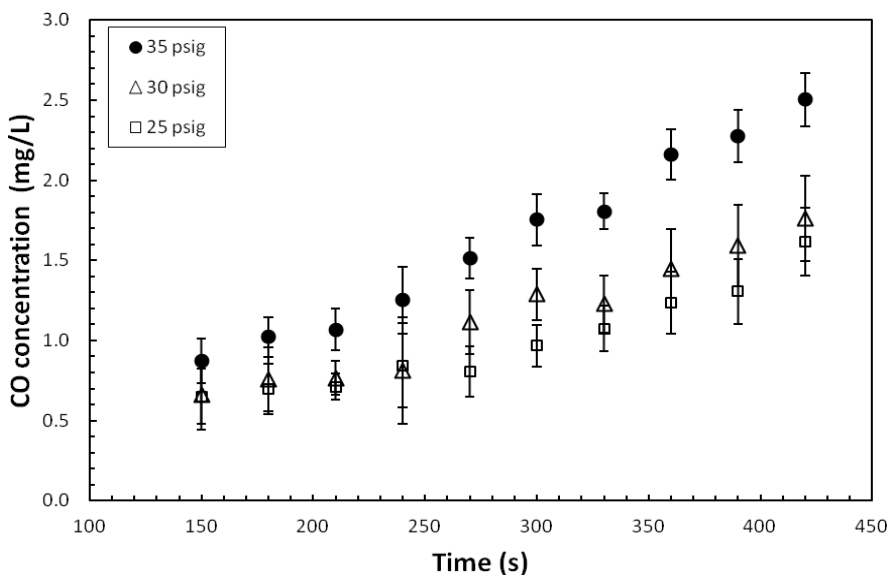

Figure 4.8. Carbon monoxide concentration profile for composite hollow fiber (CHF) membrane reactor

Theoretically, the mass transfer of the membrane reactor can be improved by a continuous utilization of the diffused CO by the microorganisms. Therefore, use of the microorganisms capable of utilizing gaseous substrates such as CO might improve the mass transfer in CHF membrane reactors.

4.2.3 Statistical validation

In order to validate the results obtained during this study, the data were analyzed using SAS. Duncan's multiple range test and Bonferroni t test were carried out to rank the reactors according to their significance in terms of mass transfer efficacy. Table 4.1 summarizes the ranking of different reactors according to Duncan groups (similar results were also obtained from Bonferroni t tests). The air-lift combined with a 20-μm bulb diffuser showed the highest mean value for dissolved CO concentration. Thus, statistically, there was no significant difference between the air-lift reactor combined with a 20-μm bulb diffuser and the reactor with only a 20-μm bulb diffuser.

Table 4.1. Reactor ranking according to Duncan grouping

Groups*	Reactor configurations	Mean value**	N***
A	Air-lift combined with a 20-μm bulb diffuser	19.69	30
BA	20-μm bulb diffuser	19.37	30
B	Column diffuser	19.07	30
C	Sparger with mixer (150 rpm)	18.41	30
D	Air-lift combined with a single gas entry point	17.52	30
D	Sparger only	17.35	30
D	Sparger with mixer (300 rpm)	17.04	30

* Refer to the Duncan groups, ** CO concentration in liquid phase (mg/L), *** N: Sample size.

4.3 CO and H_2 Mass Transfer Using Composite Hollow Fiber (CHF) Membrane Reactor

4.3.1 CO mass transfer using CHF membrane module

CO concentration in the liquid samples extracted from the reactor for various flow rates and inlet pressure values were determined using Mb-protein bioassay. The CO concentration in the liquid phase increased with the liquid recirculation flow rate and the CO inlet pressure. Three trials for each operating condition were conducted and an average mass transfer coefficient was calculated to minimize potential experimental errors. The theoretical CO saturation concentration in an aqueous phase at room temperature and atmospheric pressure was reported around 26.6 mg/L (Bredwell and Worden, 1998). However, in this study the maximum CO concentration of 15 mg/L was achieved under a recirculation flow rate of 1500 mL/min and CO inlet pressure of 30 psig. During the experiment, none of the operational runs reached the CO saturation concentration within the reactor. The CHF membrane had the advantage of operating under high inlet gas pressures without forming CO bubbles (Lee and Rittmann, 2001; Nerenberg and Rittmann, 2004).

Once the CO concentration in the liquid phase was determined, the variation of $ln\ (C^*/(C^*-C_1))$ with time was plotted. In this case, C^* (the liquid phase CO saturation concentration in equilibrium with the gas phase) was determined using Henry's law for each inlet pressure (Ahmed and Semmens, 1992). According to eq. (3.14), the gradient of the plot was equal to $(Q/V)\ (1-exp\ (-KaL/v_L))$. Table 4.2 summarizes the overall volumetric mass transfer coefficient (*Ka*) values obtained for the various operational conditions of this study. The maximum *Ka* value of 946.6±46.4 1/h was observed at 30 psig CO inlet pressure and 1500 mL/min liquid recirculation flow rate. The minimum *Ka* value of 85.7±8.0 1/h was obtained under 5 psig and 300 mL/min recirculation flow rate.

Table 4.2. Overall volumetric mass transfer coefficients (*Ka*) obtained using CO for various operational conditions

Pressures (psig)	Recirculation flow rates (mL/min)	*Ka* (1/h)	Pressures (psig)	Recirculation flow rates (mL/min)	*Ka* (1/h)
5 (34.5 kPa_g)	300	85.7±8.0	20 (137.9 kPa_g)	300	150.4±17.2
	600	114.3±13.4		600	293.2±23.1
	900	133.1±17.4		900	437.0±13.2
	1200	149.1±19.4		1200	629.7±54.2
	1500	205.0±16.2		1500	824.4±42.9
10 (68.9 kPa_g)	300	115.0±12.2	25 (172.4 kPa_g)	300	158.2±14.6
	600	144.4±16.5		600	334.9±20.8
	900	225.8±14.2		900	530.2±21.7
	1200	288.4±21.9		1200	746.9±30.6
	1500	383.0±18.1		1500	939.5±43.2
15 (103.4 kPa_g)	300	137.6±16.1	30 (206.8 kPa_g)	300	157.2±15.1
	600	242.7±11.2		600	366.4±27.9
	900	344.4±23.8		900	586.5±26.4
	1200	489.5±29.2		1200	784.3±58.0
	1500	642.7±35.2		1500	946.6±46.4

The overall *Ka* values reported in many studies (similar to the k_La values reported in Table 2.3) are lower than this study. Most of the previous studies were conducted using completely mixed reactors and the mass transfer was controlled by the mixing speeds of the agitators. However, this is not economically attractive in commercial syngas fermentation due to high energy consumption. Therefore, according to the findings of this study, it is evident that the use of CHF membranes improves mass transfer effectively.

4.3.2 H_2 mass transfer using CHF membrane module

H_2 mass transfer experiments were conducted following the procedure described in section 3.6.2. Table 4.3 shows the *Ka* values obtained for H_2 using the CHF membrane reactor. A lower *Ka* value was observed for H_2 than the CO. The maximum *Ka* value of

544.6 ±18.41/h was obtained for H_2 at 30 psig and 1500 mL/min, while the minimum was recorded as 22.7±1.6 1/h at 5 psig and 300 mL/min. Bredwell et al. (1999) reported a maximum *Ka* value of 335 1/h for H_2 using a lab-scale trickle bed reactor. However, the feasibility of scaling up the trickle bed reactor is a challenge. Therefore, it is very important to have both higher mass transfer and a better scalability for industrial applications.

Table 4.3. Overall volumetric mass transfer coefficient (*Ka*) values obtained for H_2 using CHF membrane reactor

Pressures (psig)	Recirculation flow rates (mL/min)	*Ka* (1/h)	Pressures (psig)	Recirculation flow rates (mL/min)	*Ka* (1/h)
5 (34.5 kPa_g)	300	22.7±1.6	20 (137.9 kPa_g)	300	71.2±6.5
	600	42.3±3.9		600	117.2±10.4
	900	52.5±5.3		900	210.5±5.6
	1200	60.4±6.2		1200	274.5±10.2
	1500	70.3±6.4		1500	333.8±14.4
10 (68.9 kPa_g)	300	32.2±2.6	25 (172.4 kPa_g)	300	94.9±6.9
	600	62.4±5.8		600	187.5±8.2
	900	83.9±8.2		900	293.4±9.3
	1200	99.9±6.2		1200	374.7±11.8
	1500	121.0±7.8		1500	466.5±14.5
15 (103.4 kPa_g)	300	57.3±4.6	30 (206.8 kPa_g)	300	112.2±8.3
	600	78.4±5.4		600	172.7±10.7
	900	119.4±7.4		900	285.9±11.5
	1200	179.0±9.2		1200	409.5±23.4
	1500	258.7±14.5		1500	544.6±18.4

4.3.3 Mixed syngas mass transfer using CHF membrane module

Mixed syngas mass transfer experiments were conducted using the CHF membrane module and a customized syngas mixture of 20% CO, 10% H_2, 15% CO_2 and 55% N_2. Different inlet pressures were used in the analysis including 10, 20 and 30 psig. Liquid samples were collected at an interval of one minute for CO and H_2 analysis. In this case, Mb-protein bioassay and GC-TCD methods were used to determine the CO and H_2 concentrations, respectively, in the aqueous phase. Table 4.4 shows the volumetric mass transfer coefficients obtained during the experiment.

Table 4.4. Overall volumetric mass transfer coefficients (*Ka*) obtained for mixed syngas analysis

Membrane types	Inlet gas pressures (psig)	Recirculation flow rates (mL/min)	*Ka* values (1/h)	
			CO	H_2
MHF0504 MBFT	10	800	46.8±2.8	4.6±0.2
		1600	73.9±4.7	15.8±0.6
	20	800	54.7±3.9	14.7±0.8
		1600	113.4±6.4	26.7±1.3
	30	800	104.3±3.8	17.4±0.4
		1600	152.2±9.8	42.6±2.8

The *Ka* values obtained in the mixed syngas analysis were in the range of 8% for H_2 to 18% for CO of the *Ka* values reported in individual H_2 and CO mass transfer experiments, respectively (Tables 4.2 and 4.3). This was mainly because of the low percent of each component gases (CO and H_2) in the syngas mixture. In this case, the gas compositions were 20% CO, 10% H_2, 15% CO_2 and 55% N_2. Moreover, a reduction in *Ka* value was observed with the increasing inlet gas pressure. Gas stripping could be a possible reason for this phenomenon (Kopke et al., 2011).

4.4 Model Development and Validation

4.4.1 Model development

4.4.1.1 Development of the model using CO mass transfer data

Developing models are extremely important when it comes to scale-up bench scale studies. Therefore, in the case of CO mass transfer using CHF membranes operated under various pressures, it is important to develop a non-dimensional relationship between the operating pressure and the other parameters such as recirculation flow rate, diameter, length and surface area of the membrane fibers, and liquid velocity through the fibers. A model equation was developed for CO mass transfer using the theoretical equations described in section 3.6.2. Figure 4.9 presents the variation of Sherwood number (*Sh*) with the Reynolds number (*Re*) for various pressure values. In this study, the 1/3 power dependent of the Schmidt number (*Sc*) was assumed in mass transfer correlations (Cussler, 1984).

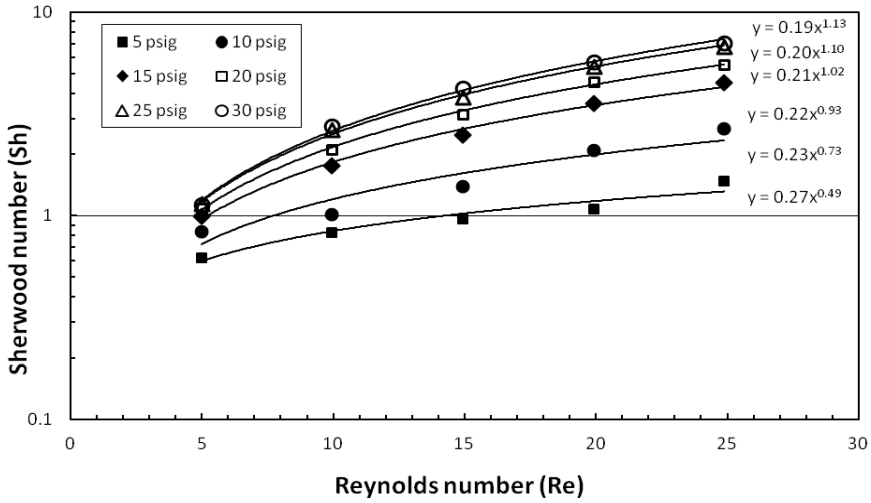

Figure 4.9. Variation of Sherwood number with Reynolds number for various pressure values

The power trend line fitting of the data yields the following relationships at various pressure values as given by eqs. (4.1) - (4.6).

5 psig	$Sh=0.04\ Re^{0.49}\ Sc^{0.33}$	(4.1)
10 psig	$Sh=0.03\ Re^{0.76}\ Sc^{0.33}$	(4.2)
15 psig	$Sh=0.03\ Re^{0.94}\ Sc^{0.33}$	(4.3)
20 psig	$Sh=0.03\ Re^{1.05}\ Sc^{0.33}$	(4.4)
25 psig	$Sh=0.03\ Re^{1.11}\ Sc^{0.33}$	(4.5)
30 psig	$Sh=0.03\ Re^{1.13}\ Sc^{0.33}$	(4.6)

According to the relations derived above, it is clear that both coefficients and the exponents are pressure dependent. Further, the coefficient and the exponent are likely to reach their minimum and maximum values, respectively, beyond 30 psig. According to the statistical analysis, there was no significant difference in mass transfer characteristics between the pressure values of 25 and 30 psig. Figure 4.10 shows the variation of the coefficient and the exponent of the above relationships with pressure as shown in eqs. (4.1) - (4.6).

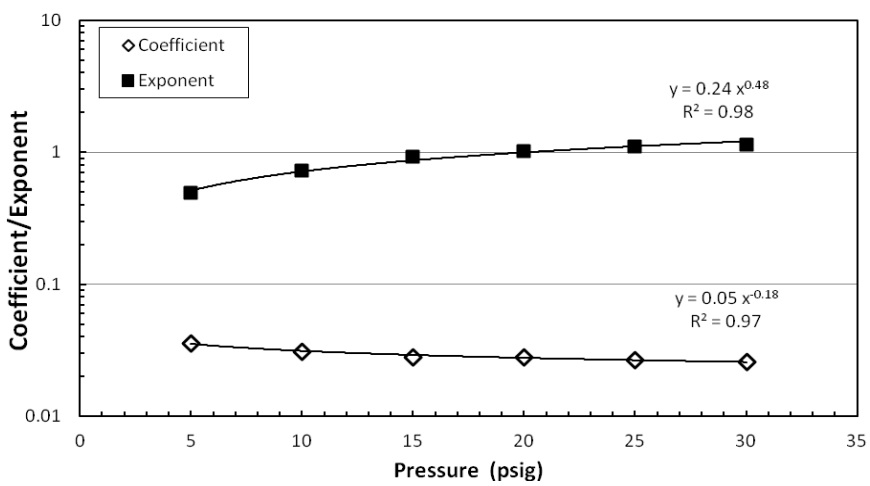

Figure 4.10. Variation of the coefficient and the exponent at different pressure values

A regression analysis of coefficients and the exponents further gives a modeling equation which can be used in scaling up the membrane bioreactor system with enhanced mass transfer properties (eq. (4.7)).

$$Sh = 0.05\, P^{-0.20} Re^{0.24\, P^{0.48}} Sc^{0.33} \tag{4.7}$$

Where, *P* is the inlet CO pressure in psig. Eq. (4.7) can be used to predict the mass transfer characteristics in a CHF membrane module with outside-in configuration for pressures between 5 to 30 psig and the Reynolds numbers between 5 and 35. Table 4.5 shows a comparison of mass transfer correlations found in the literature. There is a strong correlation between the data published in the literature and this study, especially when the flow is in the laminar range (Re<2300). These analytical model equations are highly depended on reactor configuration and the flow pattern, type of membrane, type of gas and the liquid. Therefore, it is important to select the appropriate model for scale up purposes.

One of the major advantages of CHF membrane is that it can be operated at high pressures. The higher pressures increase the CO mass transfer significantly. In this case, the membrane resistance was comparatively less, allowing the CO mass transfer to occur at its maximum efficiency. Therefore, these CHF membranes have a great potential of improving mass transfer in syngas fermentation and other similar applications such as wastewater treatments and syngas to methane conversions.

Table 4.5. Comparison of mass transfer correlation equations from literature

Correlation equations	Flow geometries	Flow ranges	References
$Sh = 0.02\, Re^{0.60} Sc^{0.33}$	n/a	n/a	Knudsen and Katz, 1958
$Sh = 0.39 Re^{0.59} Sc^{0.33}$	Flow outside and across fibers (for O_2)	Re>2.5	Wikramasinghe et al., 1992
$Sh = 0.12 Re^{1.0} Sc^{0.33}$	Flow outside and across fibers (for O_2)	Re<2.5	
$Sh = 1.62 \left(Re \frac{d}{l}\right)^{0.33} Sc^{0.33}$	Flow inside fibers (for O_2)	Gr^*>4	
$Sh = 0.02 \left(Re \frac{d}{l}\right)^{1.0} Sc^{1.0}$	Flow outside and parallel to fibers(for O_2)	Gr^*<4	
$Sh = 1.25 \left(Re \frac{d_e}{l}\right)^{0.93} Sc^{0.33}$	n/a	5<Re<3500	Yang and Cussler, 1986
$Sh = 0.61 Re^{0.36} Sc^{0.33}$	Flow outside and gas inside fibers (for O_2)	n/a	Cote et al., 1988
$Sh = 0.01 Re^{0.81} Sc^{0.33}$		600<Re<46000	Ahmed and Semmens, 1992
$Sh = 0.06\, P^{0.73} Re^{0.64\, P^{-0.22}} Sc^{0.33}$		2500<Re<5500	Ahmed et al., 2004
$Sh = 0.05\, P^{-0.20} Re^{0.24\, P^{0.48}} Sc^{0.33}$	Flow inside fibers (for CO)	5<Re<35	Current study

[*] Graetz number $Gr = d^2 v/Dl$; Sherwood number $Sh = kd/D$; Reynolds number $Re = dv/\nu$; Schmidt number $Sc = \nu/D$

Note: d is the fiber diameter and d_e is the effective diameter.

4.4.1.2 Membrane resistance analysis

Mass transfer between the gas and the liquid phases mainly depends on the driving force (such as pressure, concentration and temperature differences) between the two phases. In this case, the concentration gradient between the two phases acts as the driving force that result an effective mass transfer.

As described in section 3.6.2, membrane resistance ($1/Hk_U$) can be determined by plotting the reciprocal of observed mass transfer coefficient ($1/K$) and the reciprocal of the liquid velocity ($1/v_L$) (Ahmed et al., 2004). After plotting the variations for different CO inlet pressures and recirculation flow rates, the membrane resistance was obtained as 1.4±0.2 min/cm. Therefore, the mass transfer coefficient of the non-porous polyurethane layer of the CHF membrane was 0.7±0.1 cm/min. Ahmed et al. (2004) reported a membrane resistance of 38.2 cm/min for their membrane system. The membrane resistance is highly depends on membrane properties such as porosity, pore sire, surface area, operational mode (dead –end or cross-flow) and the material of the membrane fibers. The observed high mass transfer coefficient for the non-porous layer of the membrane was a direct consequence of the outside-in (water flowing inside the fiber lumen) reactor configuration. In this study the membrane resistance showed a minimum effect on CO mass transfer. Resistance due to the liquid boundary layer inside the fiber lumen accounted for about 90 to 95% of the total mass transfer resistance. This might be attributed to low flow velocities through the membrane fibers. Therefore, further investigation is necessary to determine the effects of the high liquid velocities (for higher *Re* numbers) and mass transfer properties.

4.4.1.3 Statistical validation

The data obtained in this study was validated using several statistical models (in SAS). A Duncan's multiple range and Bonferroni t-tests were carried out to determine the significance of CO inlet pressure and recirculation flow rates. The α value was selected as 0.05 for all statistical analysis models. During the analysis, it was observed that the selected pressure values and recirculation flow rates have a significant effect on the volumetric mass transfer coefficient.

Further, the pressure values (5 to 30 psig) were ranked according to their significance using Duncan's method. The results showed that the pressure values from 5 to 20 psig can be categorized into four different Duncan groups, while the other two pressure values (25 and 30 psig) into one group. This means that statistically, there was no significant difference in *Ka* values obtained for pressure values of 25 and 30 psig. This confirms the results obtained in Figure 4.9.

4.4.1.4 Development of the model using H_2 mass transfer data

Once the mass transfer data was obtained, the model was developed using the model equations described in section 3.6. Figure 4.11 shows the Sherwood number (*Sh*) as a function of Reynolds number (*Re*).

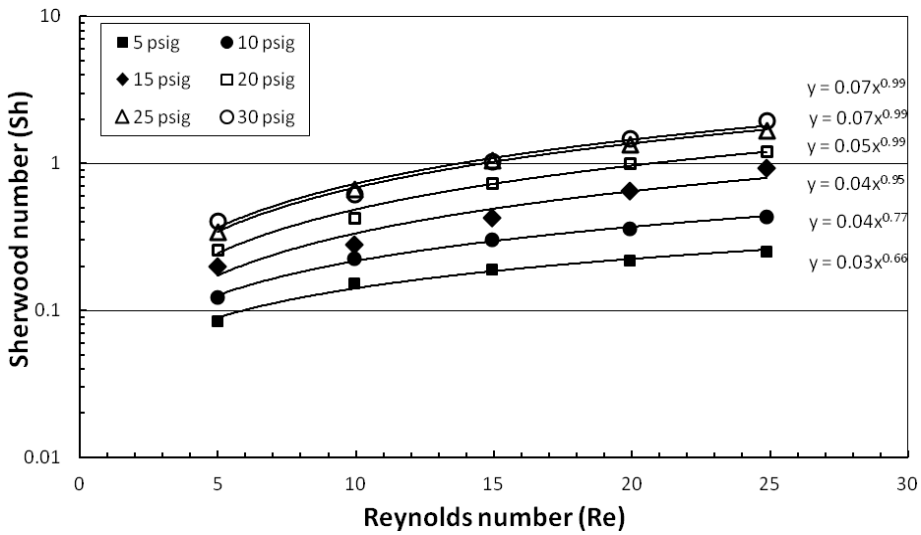

Figure 4.11. Variation of Sherwood number (*Sh*) and Reynolds number (*Re*) for H_2

The power trend line regression analysis on the data yields the following equations (eqs. (4.8)-(4.13)).

5 psig $$Sh=0.53*10^{-2}\ Re^{0.66}\ Sc^{0.33} \quad (4.8)$$

10 psig $$Sh=0.63*10^{-2}\ Re^{0.77}\ Sc^{0.33} \quad (4.9)$$

15 psig $$Sh=0.63*10^{-2}\ Re^{0.95}\ Sc^{0.33} \quad (4.10)$$

20 psig $$Sh=0.86*10^{-2}\ Re^{0.99}\ Sc^{0.33} \quad (4.11)$$

25 psig $$Sh=1.18*10^{-2}\ Re^{0.99}\ Sc^{0.33} \quad (4.12)$$

30 psig $$Sh=1.26*10^{-2}\ Re^{0.99}\ Sc^{0.33} \quad (4.13)$$

According to the above relationships, the coefficient and the exponent of *Re* reaches its maximum values after 25 psig. A similar situation was observed in the case of CO mass transfer model development. Figure 4.12 shows the variation of these coefficients/exponents with the H_2 gas pressures.

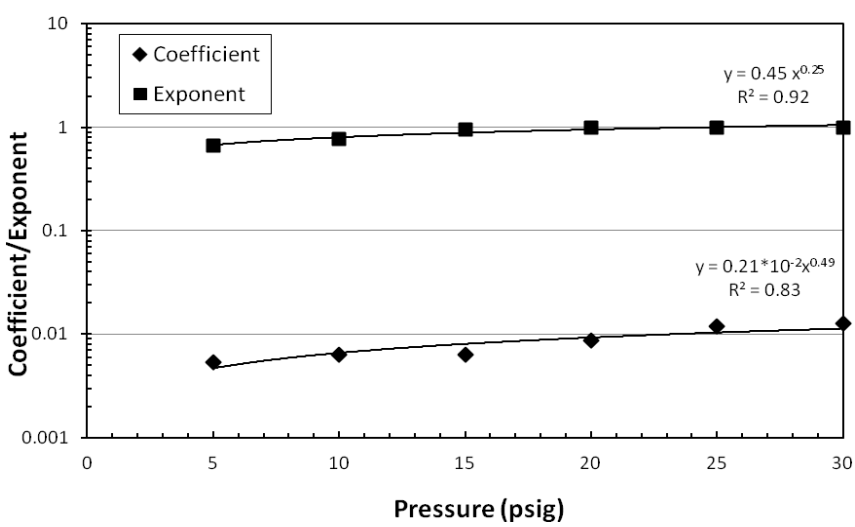

Figure 4.12. Variation of coefficient/exponent with H_2 gas pressures

In order to obtain the final model equation from the above data, a regression analysis was performed (eq. (4.14)). However, the coefficient of Re in eq. (4.14) was around 3-folds smaller than the model developed for CO (eq. (4.7)) for a given pressure. This phenomenon was partially reflected in the overall *Ka* values obtained for H_2.

$$Sh = 0.21 * 10^{-2} * P^{0.49} Re^{0.45\, P^{0.25}} Sc^{0.33} \qquad (4.14)$$

Where, *P* is the inlet H_2 pressure in psig. The above model equation was developed for pressure between 5 and 30 psig and *Re* between 5 and 35.

4.4.2 Validation of the model

In order to test the developed models for CO and H_2, two different membrane modules (PDMSXA-2500 and PDMSXA-8300) were selected. The operational parameters and details of the membrane materials are listed in Table 3.3. In this case, the membrane modules were examined under three different pressure values and three recirculation flow rates. For example, the PDMSXA-2500 membrane module was operated under the pressure values of 10, 15 and 20 psig and the recirculation flow rates of 400, 800 and 1600 mL/min. Table 4.6 compares the *Ka* values obtained from the experiments (Ka_{exp}) and the values obtained from the model (Ka_{model}) developed during the mass transfer analysis for CO. A good agreement between the Ka_{exp} and the Ka_{model} values were observed, especially at low pressures. Once the pressure started to increase beyond 30 psig, the deviation between the Ka_{exp} and Ka_{model} also started to grow. In this case, the analytical model was developed using the pressure values varying between 5 and 30 psig. This could be the likely reason for the drastic variations of the Ka_{exp} and Ka_{model} values beyond 30 psig.

Table 4.6. Comparison of overall volumetric mass transfer coefficient (*Ka*) values obtained using different membrane modules from the experiment (Ka_{exp}) and the model (Ka_{model}) for CO

Membrane types	Pressures (psig)	Flow rates (mL/min)	*Ka* values (1/h)		Ka_{model} / Ka_{exp}
			Ka_{exp}	Ka_{model}	
PDMSXA-2500	10	400	100.3±7.2	85.8	0.86
		800	180.2±9.4	141.8	0.79
		1600	343.2±16.8	234.4	0.68
	15	400	130.5±5.2	121.2	0.93
		800	286.0±11.3	223.0	0.78
		1600	536.5±42.1	410.6	0.77
	20	400	140.5±4.8	163.4	1.16
		800	376.4±11.6	329.3	0.87
		1600	795.7±55.4	663.5	0.83
PDMSXA-8300	10	400	136.0±5.3	173.9	1.28
		800	279.1±9.2	287.4	1.03
		1600	427.9±19.5	475.0	1.11
	20	400	190.8±10.3	234.9	1.23
		800	398.7±28.7	473.4	1.19
		1600	816.2±41.5	953.9	1.17
	40	400	198.2±12.3	377.4	1.90
		800	695.7±52.1	1002.9	1.44
		1600	1269.2±84.2	2664.9	2.10

Similar results were observed when compared the Ka_{exp} and Ka_{model} values obtained for H_2 (Table 4.7). Further, the *Ka* values obtained in the study for H_2 were nearly half of the *Ka* values obtained during the CO mass transfer analysis. This was true in all the mass transfer experiments conducted during the study. In fact, this was confirmed by previous publications (Kopke et al., 2011, Datar et al., 2004).

Table 4.7. Comparison of overall volumetric mass transfer coefficient (*Ka*) values obtained using different membrane modules from the experiment (Ka_{exp}) and the model (Ka_{model}) for H_2

Membrane types	Pressures (psig)	Flow rates (mL/min)	*Ka* values (1/h)		Ratio of Ka_{model} / Ka_{exp}
			Ka_{exp}	Ka_{model}	
PDMSXA-2500	10	400	46.3±2.1	34.7	0.75
		800	71.6±4.7	60.3	0.84
		1600	117.4±9.3	105.1	0.89
	15	600	79.2±4.3	53.4	0.67
		800	115.6±6.6	98.6	0.85
		1600	209.4±14.7	182.2	0.87
	20	400	95.0±4.9	73.6	0.77
		800	166.6±12.5	142.4	0.85
		1600	334.8±19.3	275.4	0.82
PDMSXA-8300	10	400	50.3±4.8	64.1	1.28
		800	80.6±6.9	111.7	1.39
		1600	147.4±12.1	194.5	1.32
	20	400	94.2±7.2	113.7	1.21
		800	185.6±16.7	219.8	1.18
		1600	349.4±31.9	425.1	1.22
	40	400	162.0±15.2	210.5	1.30
		800	271.6±24.5	461.2	1.76
		1600	594.8±56.4	1010.5	1.70

The differences in membrane properties such as membrane surface area, fiber length and material might have significant implications for these variations between the *Ka* values. For example, PDMSXA membranes were made of silicon and they showed different affinities to various liquids and gases. Therefore, selecting a membrane module for a specific application could be time consuming. However, using appropriate models, the most suitable membrane modules could be selected.

In this case, the developed models for CO and H_2 were able to predict the volumetric mass transfer coefficients with an accuracy of nearly, 85%. That means the developed models could be used in syngas fermentation applications with enhanced mass transfer properties. Further, these models could be used in reactor scale-up, using CHF membrane modules.

CHAPTER 5

ENGINEERING IMPLICATIONS

Gas-liquid mass transfer limitation is one of the major issues in many biological systems. In syngas fermentation, this is considered to be the major bottle-neck, preventing the commercialization of the process. On the other hand in wastewater treatment facilities, aeration is one of the major cost-intensive unit operations. Therefore, innovative reactor designs which are able to enhance the gas-liquid mass transfer could be an important contribution.

Composite hollow fiber (CHF) membranes have been adopted in hydrogen and oxygen mass transfer in water and wastewater treatment applications. However, the use of CHF membranes for mass transfer in syngas fermentation is an innovative approach which offers several advantages over the conventional bioreactors. Densely packed hollow fibers, micro-porous membrane surface (< 1μm), non-porous thin composite layer and hydrophobic polymer coating are the key performance parameters of CHF membranes. In this study, a new reactor configuration consisting of a CHF membrane module was examined, in order to enhance the gas-liquid mass transfer.

The highest overall volumetric mass transfer coefficient (*Ka*) of 950 1/h for CO was observed using the CHF membrane reactor. The average *Ka* value required for an industrial-scale syngas fermentation facility was reported as 580 1/h. Therefore, the CHF membrane reactor developed in this study has a great potential to be used in industrial-scale syngas fermentation.

Further, the CHF reactor developed in this study could be used in various other gas-liquid mass transfer applications such as syngas to methane, syngas to carboxylic acid and syngas to biopolymer and other biochemical productions.

5.1 Example of CHF Membrane Reactor Design Calculation

Determine the number of membrane modules needed to achieve an overall mass transfer coefficient (*Ka*) of 1100 1/h for CO using water as the liquid phase. The reactor will be operated at a CO inlet pressure of 30 psig and *Re* of 25. In this case, the given hydrophobic polyethylene composite hollow fiber (CHF) membrane module has the following dimensions:

Surface area of the fibers	$=A_1$ cm^2
External fiber diameter	$= d_1$ cm
Number of fibers per module	$= N$
Length of the membrane fibers	$= L$ cm
Diameter of the membrane module	$= d_2$ cm

The model equation is given in eq. (4.7),

$$Sh = 0.05\, P^{-0.20} Re^{0.24\, P^{0.48}} Sc^{0.33} \qquad (4.7)$$

Where, *P* is the gas inlet pressure (psig), *Re* is the Reynolds number, *Sc* is the Schmidt number and *Sh* is the Sherwood number.

<u>Mass transfer calculation</u>

From eqs. (3.15), (3.16) and (3.17)

$$Sh = \frac{Kd}{D} \qquad (3.15)$$

$$Re = \frac{v_L d}{\nu} \qquad (3.16)$$

$$Sc = \frac{\nu}{D} \qquad (3.17)$$

Where, K is the overall mass transfer coefficient (1/h), d is the membrane fiber internal diameter (cm), D is the diffusivity coefficient (m^2/s), v_L is the liquid velocity through the membrane fibers (cm/s), v is the kinematic viscosity (m^2/s). In this case, for water, D=2.23x10^{-5} cm^2/s and v=9 x10^{-3} cm^2/s.

Therefore, substituting v and D in eq. (3.17),

$$Sc = 403.59$$

Substituting pressure (P) of 30 psig, Reynolds number (Re) of 25 and Sc in eq (4.7),

$$Sh = 4.7$$

From eq. (3.15),

$$K = 23.58 \text{ cm/h}$$

Therefore, the membrane specific surface area (a) needed to obtain a Ka of 1100 1/h

$$a = 46.7 \text{ 1/cm}$$

<u>Membrane module calculations</u>

Total volume of the membrane module $= \frac{\pi d_2^2}{4} * L$

Total volume of the membrane fibers $= \frac{\pi d_1^2}{4} * L * N$

Therefore, the volume of the membrane module $= \frac{\pi}{4} L(d_2^2 - d_1^2 * N)$

Then the specific surface area of the membrane (a) $= \frac{A_1}{\frac{\pi}{4} L(d_2^2 - d_1^2 * N)}$

Therefore, the number of membrane modules needed $= \frac{a_{required}}{a_{module}} = \frac{46.7}{\left[\frac{A_1}{\frac{\pi}{4} L(d_2^2 - d_1^2 * N)}\right]}$

CHAPTER 6

CONCLUSIONS

Based on the findings of this research, the following conclusions can be drawn.

1. In this study, myoglobin (Mb) - protein bioassay was used to determine the CO concentration in the aqueous phase. The study reveals a good correlation (R^2=0.97) between the two CO determining techniques, namely myoglobin (Mb)-protein bioassay and gas chromatography (GC-TCD) method.

2. A side-by-side comparison of carbon monoxide mass transfer coefficient (k_La) in eight different reactor configurations including a column diffuser, a 20-μm bulb diffuser, gas sparger, gas sparger with mechanical mixing, submerged composite hollow fiber (CHF) membrane module, air-lift combined with a 20-μm bulb diffuser, and gas-lift combined with a single gas entry point was conducted. The highest k_La value of 91.1±5.3 1/h was observed for CO using the gas-lift reactor combined with a 20-μm bulb diffuser.

3. The maximum *Ka* values of 946.6±46.4 and 544.6±18.4 1/ h were recorded for CO and H_2, respectively, using a CHF membrane reactor. Further, the model equations: $Sh=0.05\ P^{-0.22}Re^{0.24\ P^{0.48}}Sc^{0.33}$ and $Sh=0.21*10^{-2}*P^{0.49}Re^{0.45\ P^{0.25}}Sc^{0.33}$ for CO and H_2, respectively, were developed using the same reactor.

4. The validation of the model was conducted using polydimethyl siloxane (PDMSXA-2500 and PDMSXA-8300) membrane modules. It was observed an acceptable agreement between the $Ka_{\exp}$ and Ka_{model} values, with a reliability of nearly, 85%.

CHAPTER 7
FUTURE WORKS

In this study, three main hypotheses were clarified within the stipulated time frame. However, some of the hypotheses need further investigation.

- In this study, the gas-liquid mass transfer analysis was conducted using water as the liquid phase. However, in syngas fermentation microbial cultures are used as biocatalyst. Therefore, a detailed study on gas-liquid mass transfer using microbial culture media requires to be investigated.

- Several mass transfer models (without culture media) had been developed in this study. However, the effects of the microbial culture with developed models were not investigated during the current study. Therefore, the implications of the developed models with microbial culture media need to be investigated.

- Issues related to gas-liquid mass transfer limitations are common in biological systems. Therefore, the application of CHF membrane reactor in other biological systems such as syngas to methane, syngas to carboxylic acid, and syngas to biopolymer conversions needs to be investigated.

APPENDIX A

PICTURES OF EXPERIMENTAL SET-UPS AND MEMBRANE MODULES

Figure A.1. Experimental set-up with mechanical mixing

Figure A.2. Experimental set-up with gas-lift reactor combined with 20-µm bulb diffuser

Figure A.3. Experimental set-up with composite hollow fiber (CHF) membrane module

Figure A.4. Liquid sampling from the CHF membrane reactor

Figure A.5. Experimental set-up with PDMSXA-8300 membrane module

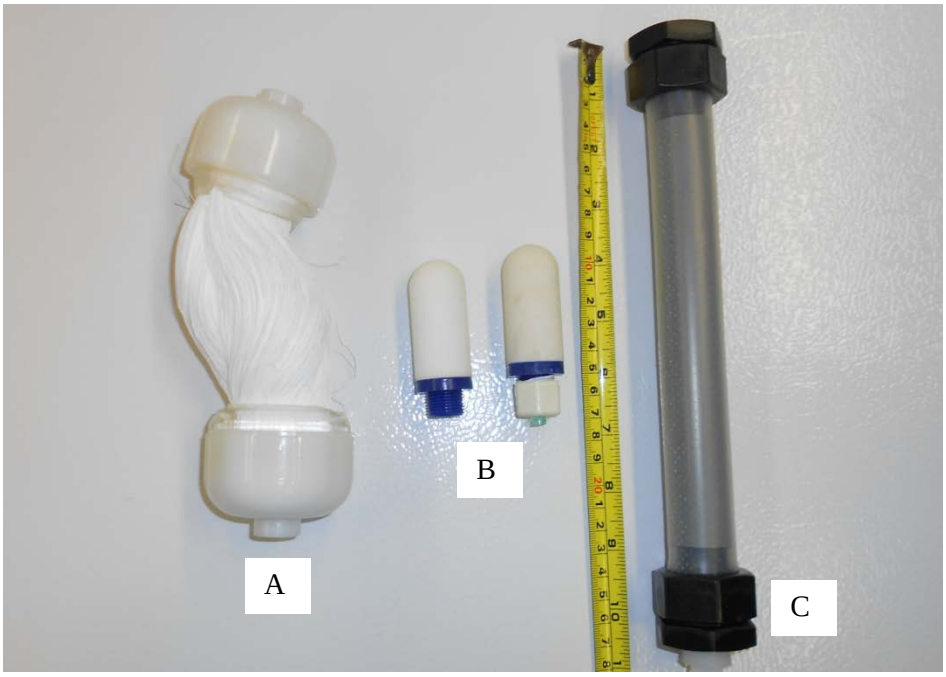

Figure A.6. Various types of diffusers used in the experiment A) CHF membrane module; B) 20-µm bulb diffuser; C) Column diffuser

APPENDIX B

CO AND H_2 CONCENTRATIONS IN THE LIQUID PHASE AND $ln\ [(C_i-C_0)/(C_i-C)]$ VALUES FOR VARIOUS REACTOR CONFIGURATIONS

Table B.1. CO concentration and $ln\ [(C_i-C_0)/(C_i-C)]$ values for sparger only reactor

Time (s)	CO flow rate 2 L/min	$ln\ [(C_i-C_0)/(C_i-C)]$	CO flow rate 3 L/min	$ln\ [(C_i-C_0)/(C_i-C)]$	CO flow rate 4 L/min	$ln\ [(C_i-C_0)/(C_i-C)]$	CO flow rate 5 L/min	$ln\ [(C_i-C_0)/(C_i-C)]$
15	3.19 ± 0.54	0.13	4.95 ± 0.55	0.21	6.23 ± 2.24	0.27	6.89 ± 0.82	0.31
30	4.25 ± 0.14	0.18	5.76 ± 0.13	0.25	10.36 ± 0.44	0.51	10.87 ± 1.62	0.54
45	8.71 ± 0.14	0.41	10.20 ± 1.29	0.50	13.18 ± 0.74	0.71	14.04 ± 1.82	0.84
60	9.52 ± 0.56	0.46	12.21 ± 1.64	0.63	14.76 ± 0.51	0.84	15.79 ± 1.43	0.93
75	11.80 ± 0.63	0.60	13.76 ± 0.25	0.75	16.68 ± 0.25	1.03	18.37 ± 1.22	1.23
90	15.00 ± 0.72	0.86	15.92 ± 0.98	0.95	18.38 ± 0.72	1.23	19.25 ± 1.51	1.35
105	14.50 ± 0.42	0.82	16.91 ± 0.24	1.05	19.23 ± 0.50	1.35	21.18 ± 0.95	1.69
120	16.56 ± 0.70	1.01	17.63 ± 0.63	1.13	19.47 ± 0.48	1.38	21.52 ± 0.60	1.76
135	16.83 ± 0.29	1.04	19.28 ± 0.95	1.35	20.84 ± 1.00	1.62	21.81 ± 1.39	1.82
150	17.08 ± 0.65	1.07	19.57 ± 0.35	1.40	19.23 ± 1.11	1.35	22.30 ± 0.41	1.95

Table B.2. CO concentration and *ln* $[(C_i-C_0)/(C_i-C)]$ values for sparger and mechanical mixing (150 rpm)

Time (s)	CO flow rate 2 L/min	*ln* $[(C_i-C_0)/(C_i-C)]$	CO flow rate 3 L/min	*ln* $[(C_i-C_0)/(C_i-C)]$	CO flow rate 4 L/min	*ln* $[(C_i-C_0)/(C_i-C)]$	CO flow rate 5 L/min	*ln* $[(C_i-C_0)/(C_i-C)]$
15	5.08 ± 0.36	0.22	5.45 ± 0.78	0.24	6.58 ± 0.65	0.29	7.85 ± 0.28	0.36
30	8.05 ± 0.67	0.37	10.09 ± 0.18	0.49	12.97 ± 1.53	0.69	14.32 ± 0.58	0.80
45	11.08 ± 1.50	0.56	13.91 ± 1.54	0.77	16.14 ± 0.67	0.97	18.34 ± 0.14	1.22
60	12.17 ± 0.68	0.63	13.38 ± 0.22	0.72	16.09 ± 0.48	0.96	16.54 ± 0.40	1.01
75	14.13 ± 0.48	0.78	17.06 ± 1.24	1.07	18.75 ± 1.05	1.28	19.39 ± 1.20	1.37
90	17.81 ± 1.75	1.15	17.63 ± 1.04	1.13	19.40 ± 1.18	1.37	20.28 ± 1.11	1.51
105	17.03 ± 1.27	1.06	18.93 ± 1.13	1.30	21.31 ± 1.36	1.71	21.91 ± 1.70	1.85
120	17.86 ± 1.20	1.16	21.51 ± 1.73	1.76	21.72 ± 1.61	1.80	22.53 ± 1.14	2.01
135	19.20 ± 1.71	1.34	20.92 ± 0.42	1.63	22.82 ± 1.56	2.10	23.42 ± 1.33	2.31
150	20.21 ± 0.08	1.50	21.88 ± 0.49	1.84	23.25 ± 0.65	2.25	23.93 ± 1.25	2.53

Table B.3. CO concentration and *ln* $[(C_i-C_0)/(C_i-C)]$ values for sparger and mechanical mixing (300 rpm)

Time (s)	CO flow rate 2 L/min	*ln* $[(C_i-C_0)/(C_i-C)]$	CO flow rate 3 L/min	*ln* $[(C_i-C_0)/(C_i-C)]$	CO flow rate 4 L/min	*ln* $[(C_i-C_0)/(C_i-C)]$	CO flow rate 5 L/min	*ln* $[(C_i-C_0)/(C_i-C)]$
15	6.13 ± 0.04	0.27	5.71 ± 0.08	0.25	8.37 ± 0.16	0.39	8.29 ± 0.90	0.38
30	10.83 ± 1.51	0.54	11.35 ± 0.99	0.57	13.22 ± 0.64	0.71	11.24 ± 0.37	0.57
45	13.16 ± 1.65	0.71	13.77 ± 0.91	0.75	15.88 ± 0.12	0.94	15.11 ± 0.18	0.87
60	14.65 ± 1.57	0.83	14.88 ± 0.08	0.85	16.21 ± 0.32	0.98	15.49 ± 0.44	0.91
75	16.11 ± 1.15	0.97	17.86 ± 0.86	1.16	21.17 ± 1.76	1.68	20.17 ± 1.35	1.50
90	16.46 ± 0.72	1.00	18.79 ± 0.93	1.28	21.30 ± 1.15	1.71	21.46 ± 1.32	1.75
105	17.32 ± 0.22	1.10	19.37 ± 1.05	1.37	21.45 ± 1.03	1.74	21.35 ± 0.11	1.72
120	18.86 ± 1.84	1.29	20.43 ± 0.53	1.54	22.66 ± 1.49	2.05	22.07 ± 1.37	1.89
135	19.87 ± 0.57	1.45	21.32 ± 0.13	1.72	23.00 ± 0.77	2.16	23.26 ± 1.12	2.25
150	21.71 ± 0.32	1.80	22.77 ± 0.09	2.09	23.42 ± 1.81	2.31	23.79 ± 0.68	2.46

Table B.4. CO concentration and $ln\ [(C_i-C_0)/(C_i-C)]$values for gas-lift reactor with 20-μm bulb diffuser

Time (s)	CO flow rate 2 L/min	$ln\ [(C_i-C_0)/(C_i-C)]$	CO flow rate 3 L/min	$ln\ [(C_i-C_0)/(C_i-C)]$	CO flow rate 4 L/min	$ln\ [(C_i-C_0)/(C_i-C)]$	CO flow rate 5 L/min	$ln\ [(C_i-C_0)/(C_i-C)]$
15	4.54 ± 0.22	0.19	6.99 ± 1.04	0.31	9.84 ± 1.11	0.48	12.29 ± 2.26	0.64
30	9.73 ± 0.97	0.47	13.17 ± 0.26	0.71	16.52 ± 0.71	1.01	19.46 ± 1.20	1.38
45	13.10 ± 0.64	0.70	16.07 ± 0.76	0.96	18.76 ± 1.45	1.28	19.72 ± 0.40	1.42
60	14.87 ± 0.46	0.85	17.22 ± 0.16	1.09	19.73 ± 0.52	1.42	20.45 ± 0.46	1.54
75	16.35 ± 1.33	0.99	19.26 ± 0.07	1.35	20.86 ± 0.34	1.62	21.00 ± 0.18	1.65
90	17.98 ± 1.50	1.18	20.36 ± 0.24	1.53	21.83 ± 0.34	1.83	22.85 ± 0.41	2.11
105	19.93 ± 0.22	1.45	21.62 ± 0.34	1.78	22.49 ± 0.72	2.00	23.91 ± 2.49	2.52
120	20.96 ± 0.70	1.64	22.91 ± 0.37	2.13	23.31 ± 0.42	2.27	24.85 ± 1.29	3.12
135	21.81 ± 1.49	1.83	23.90 ± 0.64	2.52	24.49 ± 0.55	2.85	25.39 ± 0.61	3.75
150	22.86 ± 0.32	2.11	24.46 ± 0.33	2.83	25.50 ± 0.50	3.95	25.64 ± 0.68	4.27

Table B.5. CO concentration and $ln\ [(C_i-C_0)/(C_i-C)]$ values for column diffuser

Time (s)	CO flow rate 2 L/min	$ln\ [(C_i-C_0)/(C_i-C)]$	CO flow rate 3 L/min	$ln\ [(C_i-C_0)/(C_i-C)]$	CO flow rate 4 L/min	$ln\ [(C_i-C_0)/(C_i-C)]$	CO flow rate 5 L/min	$ln\ [(C_i-C_0)/(C_i-C)]$
15	0.91 ± 0.04	0.04	3.01 ± 0.05	0.12	5.20 ± 0.24	0.22	6.46 ± 0.81	0.29
30	0.98 ± 0.04	0.04	3.89 ± 0.14	0.16	7.54 ± 0.34	0.34	9.42 ± 1.32	0.45
45	1.56 ± 0.10	0.06	5.67 ± 0.29	0.25	10.00 ± 0.73	0.49	13.33 ± 1.17	0.72
60	1.90 ± 0.06	0.08	7.53 ± 0.64	0.34	12.19 ± 0.52	0.63	15.04 ± 1.30	0.86
75	2.01 ± 0.06	0.08	9.46 ± 0.45	0.45	13.14 ± 0.55	0.70	17.03 ± 1.02	1.06
90	2.37 ± 0.02	0.10	10.36 ± 0.95	0.51	14.41 ± 0.82	0.81	18.93 ± 1.11	1.30
105	2.60 ± 0.01	0.11	11.66 ± 0.74	0.60	14.87 ± 0.80	0.85	19.37 ± 0.97	1.37
120	2.67 ± 0.07	0.11	10.53 ± 0.63	0.52	17.22 ± 1.48	1.09	19.31 ± 0.90	1.36

Table B.6. CO concentration and $ln\ [(C_i-C_0)/(C_i-C)]$values for 20-µm bulb diffuser

Time (s)	CO flow rate 2 L/min	$ln\ [(C_i-C_0)/(C_i-C)]$	CO flow rate 3 L/min	$ln\ [(C_i-C_0)/(C_i-C)]$	CO flow rate 4 L/min	$ln\ [(C_i-C_0)/(C_i-C)]$	CO flow rate 5 L/min	$ln\ [(C_i-C_0)/(C_i-C)]$
15	3.19 ± 0.54	0.13	4.95 ± 0.55	0.21	6.23 ± 2.24	0.27	6.89 ± 0.82	0.31
30	4.26 ± 0.21	0.18	5.76 ± 3.27	0.25	10.36 ± 0.68	0.51	10.87 ± 1.62	0.54
45	8.71 ± 0.14	0.41	10.20 ± 1.29	0.50	14.18 ± 0.83	0.79	14.78 ± 1.83	0.84
60	9.52 ± 0.56	0.46	12.21 ± 1.64	0.63	16.76 ± 0.92	1.03	15.79 ± 1.43	0.93
75	11.80 ± 0.63	0.60	14.76 ± 0.25	0.84	18.68 ± 0.25	1.27	18.37 ± 1.22	1.23
90	15.00 ± 0.72	0.86	16.92 ± 0.98	1.05	20.38 ± 0.72	1.53	21.25 ± 1.51	1.70
105	14.50 ± 0.42	0.82	18.91 ± 0.24	1.30	21.23 ± 0.50	1.70	22.18 ± 0.95	1.92
120	16.56 ± 0.70	1.01	19.63 ± 0.63	1.41	21.47 ± 0.48	1.75	23.52 ± 0.60	2.35
135	17.83 ± 0.29	1.16	21.28 ± 0.95	1.71	2 3.84 ± 1.00	2.49	24.81 ± 1.39	3.08

Table B.7. CO concentration and $ln\ [(C_i-C_0)/(C_i-C)]$ values for correlation study (myoglobin-protein bioassay)

Time (s)	CO flow rate 1 L/min	$ln\ [(C_i-C_0)/(C_i-C)]$	CO flow rate 2 L/min	$ln\ [(C_i-C_0)/(C_i-C)]$	CO flow rate L/min	$ln\ [(C_i-C_0)/(C_i-C)]$
8	1.89 ± 0.34	0.08	2.32 ± 0.51	0.09	4.54 ± 1.48	0.19
33	4.13 ± 0.39	0.17	6.74 ± 1.67	0.30	8.96 ± 1.64	0.42
58	6.23 ± 0.75	0.27	9.05 ± 0.65	0.43	12.65 ± 1.99	0.67
83	8.66 ± 1.45	0.40	13.92 ± 1.78	0.77	18.10 ± 1.73	1.19
108	10.26 ± 1.01	0.50	17.13 ± 2.11	1.08	21.85 ± 1.09	1.84
133	11.87 ± 1.70	0.61	20.62 ± 1.10	1.58	23.65 ± 1.12	2.40

Table B.7. (Continued) CO concentration and $ln\ [(C_i-C_0)/(C_i-C)]$ values for correlation study (myoglobin-protein bioassay)

Time (s)	CO flow rate 4 L/min	$ln\ [(C_i-C_0)/(C_i-C)]$	CO flow rate 5 L/min	$ln\ [(C_i-C_0)/(C_i-C)]$
8	6.50 ± 1.72	0.29	6.66 ± 1.28	0.30
33	12.48 ± 1.73	0.65	14.06 ± 1.07	0.78
58	17.51 ± 1.78	1.12	20.50 ± 1.16	1.55
83	21.08 ± 1.21	1.66	22.71 ± 1.78	2.07
108	22.65 ± 0.24	2.05	24.94 ± 1.97	3.20
133	24.34 ± 0.74	2.75	25.29 ± 1.16	3.60

Table B.8. CO concentration and $ln\ [(C_i-C_0)/(C_i-C)]$values used in the correlation study (gas chromatograph equipped with thermal conductivity detector)

Time (s)	CO flow rate 1 L/min	$ln\ [(C_i-C_0)/(C_i-C)]$	CO flow rate 2 L/min	$ln\ [(C_i-C_0)/(C_i-C)]$	CO flow rate 3 L/min	$ln\ [(C_i-C_0)/(C_i-C)]$
8	2.35 ± 0.68	0.09	2.27 ± 1.43	0.09	2.18 ± 1.03	0.09
33	3.49 ± 0.28	0.14	7.85 ± 1.20	0.36	14.17 ± 0.71	0.79
58	5.80 ± 0.34	0.25	13.65 ± 1.29	0.74	19.28 ± 0.98	1.35
83	9.24 ± 0.90	0.44	19.68 ± 0.62	1.41	22.55 ± 0.21	2.02
108	12.41 ± 0.66	0.65	22.45 ± 1.04	1.99	24.03 ± 0.28	2.58
133	14.88 ± 1.00	0.85	21.08 ± 0.45	1.67	24.68 ± 0.47	2.98

Table B.8. (Continued) CO concentration and $ln\ [(C_i-C_0)/(C_i-C)]$ values used in the correlation study (gas chromatograph equipped with thermal conductivity detector)

Time (s)	CO flow rate 4 L/min	$ln\ [(C_i-C_0)/(C_i-C)]$	CO flow rate 5 L/min	$ln\ [(C_i-C_0)/(C_i-C)]$
8	4.28 ± 1.41	0.18	6.64 ± 1.59	0.30
33	16.00 ± 1.81	0.96	19.90 ± 1.89	1.45
58	21.89 ± 0.88	1.85	23.76 ± 0.61	2.45
83	23.63 ± 0.41	2.39	24.99 ± 0.28	3.25
108	24.40 ± 0.28	2.79	25.48 ± 0.88	3.92
133	25.24 ± 0.19	3.53	25.67 ± 0.58	4.38

Table B.9. H_2 concentration and $ln\ [(C_i-C_0)/(C_i-C)]$ values at 30 psig pressure used in H_2 mass transfer evaluation

Time (s)	Q= 300 mL/min	$ln\ [(C_i-C_0)/(C_i-C)]$	Q= 600 mL/min	$ln\ [(C_i-C_0)/(C_i-C)]$	Q= 900 mL/min	$ln\ [(C_i-C_0)/(C_i-C)]$
15	0.062 ± 0.005	0.013	0.038 ± 0.001	0.008	0.033 ± 0.001	0.007
75	0.054 ± 0.004	0.011	0.061 ± 0.001	0.013	0.115 ± 0.005	0.025
135	0.091 ± 0.002	0.019	0.145 ± 0.005	0.031	0.229 ± 0.012	0.049
195	0.121 ± 0.011	0.026	0.219 ± 0.017	0.047	0.310 ± 0.021	0.068
255	0.182 ± 0.021	0.039	0.278 ± 0.018	0.060	0.427 ± 0.024	0.095
315	0.206 ± 0.015	0.044	0.335 ± 0.029	0.073	0.504 ± 0.033	0.112
375	0.248 ± 0.014	0.054	0.370 ± 0.021	0.081	0.602 ± 0.046	0.136
435	0.270 ± 0.022	0.059	0.424 ± 0.032	0.094	0.716 ± 0.060	0.164
495	0.319 ± 0.028	0.070	0.478 ± 0.038	0.106	0.791 ± 0.063	0.183
555	0.362 ± 0.030	0.079	0.554 ± 0.042	0.124	0.858 ± 0.068	0.200

Table B.9. (Continued) H_2 concentration and $ln\ [(C_i-C_0)/(C_i-C)]$values at 30 psig used in H_2 mass transfer evaluation

Time (s)	Q= 1200 mL/min	$ln\ [(C_i-C_0)/(C_i-C)]$	Q= 1500 mL/min	$ln\ [(C_i-C_0)/(C_i-C)]$
15	0.100 ± 0.006	0.021	0.134 ± 0.012	0.029
75	0.158 ± 0.019	0.034	0.233 ± 0.020	0.051
135	0.273 ± 0.024	0.059	0.381 ± 0.028	0.084
195	0.382 ± 0.026	0.084	0.610 ± 0.052	0.138
255	0.581 ± 0.036	0.131	0.758 ± 0.062	0.174
315	0.674 ± 0.068	0.153	0.881 ± 0.087	0.206
375	0.825 ± 0.057	0.191	1.080 ± 0.079	0.258
435	0.974 ± 0.070	0.230	1.234 ± 0.096	0.302
495	1.096 ± 0.049	0.263	1.329 ± 0.122	0.329
555	1.224 ± 0.093	0.299	1.549 ± 0.135	0.396

APPENDIX C

STANDARD CURVES USED IN THE ANALYSIS

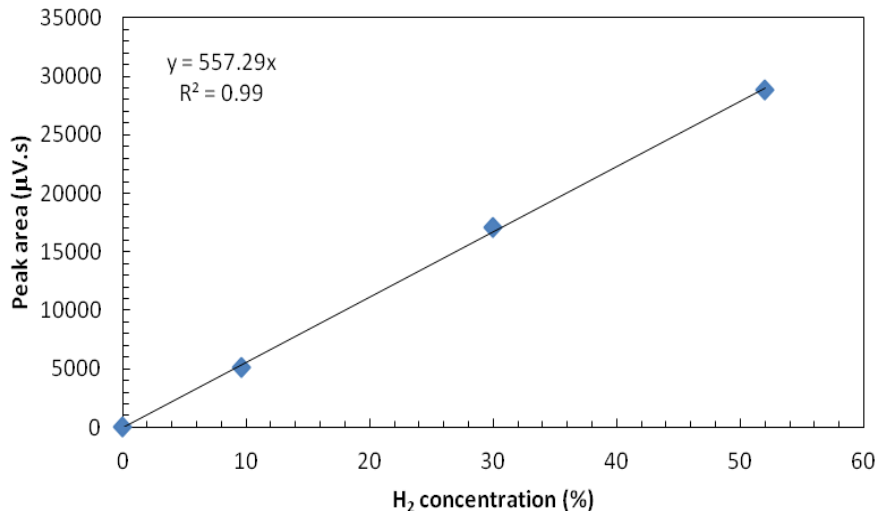

Figure C.1. Standard curve for H_2 gas measurements

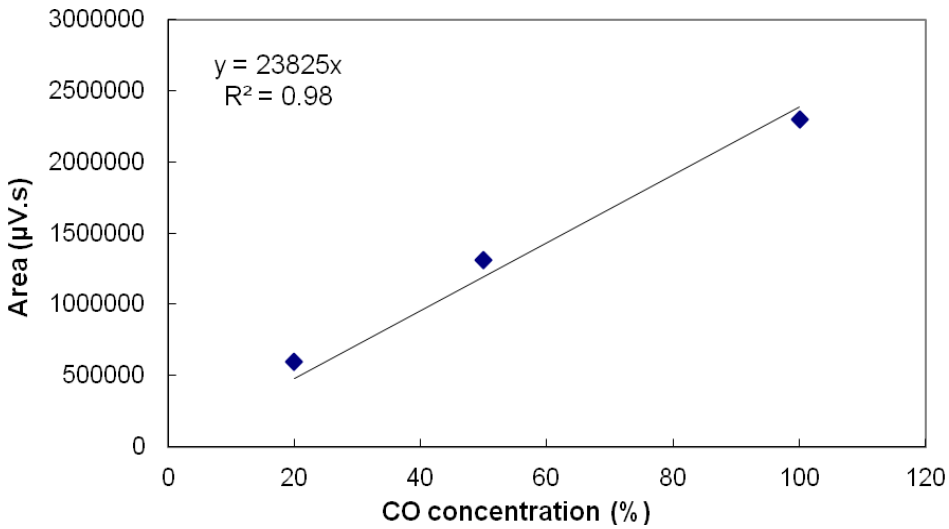

Figure C.2. Standard curve for CO gas measurements

APPENDIX D

LIST OF PUBLICATIONS

Journal Publications

Munasinghe, P.C., Khanal, S.K., 2012. Syngas fermentation to biofuel: Evaluation of carbon monoxide mass transfer and analytical modeling using a composite hollow fiber (CHF) membrane bioreactor. Bioresource Technology, 122, 130-136 (Impact factor 4.98)

Munasinghe, P.C., Khanal, S.K., 2010. Syngas fermentation to biofuel: Evaluation of CO mass transfer coefficient (k_La) in different reactor configurations. Biotechnology Progress, 26, 1616-1621 (Impact factor 2.34)

Munasinghe, P.C., Khanal, S.K., 2010. Biomass-derived syngas fermentation into biofuels: Opportunities and challenges. Bioresource Technology, 101, 5013-5022 (Impact factor 4.98)

Book Chapters

Munasinghe, P.C., Khanal, S.K., 2010. Biomass-derived syngas fermentation to biofuels (Chapter 4). Pandey, A., Larroche, C., Ricke, S.C., Dussap, C.G. (Eds). Biofuels: Alternative feedstocks and conversion processes. Elsevier Inc. USA

Conference Proceedings

Munasinghe, P.C., Khanal, S. K., 2012. Evaluation and Analytical Modeling of Carbon Monoxide Mass Transfer Using a Composite Hollow Fiber (CHF) Membrane Bioreactor in Syngas Fermentation. College of Tropical Agriculture and Human Resources (CTAHR) Symposium, April 13-14, Honolulu, HI, USA

Munasinghe, P.C., Khanal, S.K., 2011. Evaluation of hydrogen and carbon monoxide mass transfer and a correlation between myoglobin-protein bioassay and gas chromatography method for carbon monoxide determination. American Society of Agricultural and Biological Engineers (ASABE) 2011 Annual International Meeting, August 7-10, Louisville, KY, USA

Munasinghe, P.C., Khanal, S. K., 2009. Syngas fermentation to biofuel: CO mass transfer in different reactor configurations. Pacific Rim Summit on Industrial Biotechnology and Bioenergy, November 8-11, Honolulu, HI, USA

Munasinghe, P.C., Khanal, S.K., 2012. Evaluation and analytical modeling of carbon monoxide and hydrogen mass transfer using a composite hollow fiber (CHF) membrane bioreactor in syngas fermentation. International conference on Challenges in Environmental Science and Engineering (CESE) 2012, September 9-13, Melbourne, Australia

REFERENCES

Abrini, J., Naveau, H., Nyns, E.J., 1994. *Clostridium autoethanogenum*, sp. nov., an anerobic bacteriam that produces ethanol from carbon monoxide. Archives of Microbiology 161, 345-351.

Ahmed, A., Cateni, B.G., Huhnke, R.L., Lewis, S.R., 2006. Effects of biomass-generated producer gas constituents on cell growth, product distribution and hydrogenase activity of *Clostridium carboxidivorans* $P7^T$. Biomass and Bioenergy 30, 665-672.

Ahmed, A., Lewis, R.L., 2007. Fermentation of Biomass generated synthesis gas: effects of Nitric oxide. Biotechnology and Bioengineering 97 (5), 1080-1086.

Ahmed, T., Semmens, M.J., 1992. Use of sealed end hollow fibers for bubbleless membrane aeration: experimental studies. Journal of Membrane Science 69, 1-10.

Ahmed, T., Semmens, M.J., Voss, M.A., 2004. Oxygen transfer characteristics of hollow-fiber, composite membranes. Advance Environmental Research 8, 637-646.

Annual Energy outlook 2012. U.S. Energy Information Administration, Report number DOE/EIA-0383(2012), June 2012.

Biomass Research and Development Technical Advisory Committee of the U.S. Departments of Energy and Agriculture. (2002). Roadmap for Biomass Technologies in the United States, Biomass Research and Development Technical Advisory Committee.

Bouaifi, M., Hebrard, G., Bastoul, D., Roustan, M., 2001. A comparative study of gas hold-up, bubble size, interfacial area and mass transfer coefficients in gas–liquid reactors and bubble columns. Chemical Engineering and Processing 40, 97-111.

Bredwell, M. D., Worden, R. M., 1998. Mass transfer properties of microbubbles. 1. Experimental studies. Biotechnology Progress 14 (1), 31-38.

Bredwell, M.D., Srivastava, P., Worden, R.M., 1999. Reactor design issues for synthesis-gas fermentations. Biotechnology Progress 15, 834-844.

Bridgwater, A.V., 1994. Catalysis in thermal biomass conversion. Applied Catalysis A: General 116, (1-2), 5-47.

Bridgwater, A.V., 1995. The technical and economic feasibility of biomass gasification for power generation. Fuel 74, 631-653.

Britt, P. F., Buchanan, A.C., Cooney, M.J., Martineau, D.R., 2000. Flash vacuum pyrolysis of methoxy-substituted lignin model compounds. Journal of Organic Chemistry 65, 1376-1389.

Brogren, C., Karlsson, H.T., Bjerle, I., 1997. Absorption of NO in an alkaline solution of $KMnO_4$. Chemical Engineering and Technology 20(6), 396-402.

Brown, R. C., Heindel, T., Dispirito, A., Nikolau, B., 2003. Production of biopolymers and hydrogen via syngas fermentation. National ACS Meeting, Anaheim, California.

Brown, R.C., 2006. Biomass Refineries Based on Hybrid Thermochemical-Biological Processing -An Overview. Biorefineries -Industrial Processes and Products. Status Quo and Future Directions. Vol. 1 (Edited by Birgit Kamm, Patrick R. Gruber, Michael Kamm) Wiley-Vch Verlag GmbH & Co. KGaA, Weinheim.

Chakar, F.S., Ragauskas,A.J., 2004. Review of current and future softwood kraft lignin process chemistry. Industrial Crops and Products 20, 131-141.

Chang, I.S., Kim, B.H., Lovitt, R.W., Bang, J.S., 2001. Effect of CO partial pressure on cell-recycled continuous CO fermentations by *Eubacterium limosum* KIST612. Process Biochemistry 37, 411-421.

Chu, H., Chien, T.W., Li, S.Y., 2001. Simultaneous absorption of SO_2 and NO from flue gas with $KMnO_4$/NaOH solutions. Science of the Total Environment 275 (1–3), 127-135.

Coskata press release: http://www.coskata.com/company/media.asp?story=504B571C-0916-474E-BFFA-ACB326EFDB68

Cote, P.L., Bersillon, J.L., Huyard, A., Faup, J.M., 1988. Bubble-free aeration using membranes: Process analysis. Research journal of the Water Pollution Control Federation 60 (11), 1986-1992.

Cowger, J.P., Klasson, K.T., Ackerson, M.D., Clausen, E.C., Gaddy, J.L., 1992. Mass-transfer and kinetic aspects in continuous bioreactors using *Rhodspirilium rubrum*. Applied Biochemistry and Biotechnology 34/35, 613-624.

Cussler, E.L., 1984. Diffusion: Mass transfer in fluid systems, Cambridge University Press, New York, NY.

Daniel, S.L., Hsu, T., Dean, S.I., Drake, H.L., 1990. Characterization of the hydrogen- and carbon monoxide-dependent chemolithotrophic potentials of the acetogens *Clostridium thermoaceticum* and *Acetogenium kivui*. Journal of Bacteriology 172, 4464-4471.

Daniels, L., Fuchs, G., Thauer, R. K., Zeikus, J. G., 1977. Carbon monoxide oxidation by methanogenic bacteria. Journal of Bacteriology 132(1), 118-26.

Datar, R.P., Shenkman, R.M., Cateni, B.G., Huhnke, R.L., Lewis, R.S., 2004. Fermentation of biomass-generated producer gas to ethanol. Biotechnology and Bioengineering 86, 587-94

Demirbas, A., 2007. Progress and recent trends in biofuels. Progress in Energy and Combustion Science 33, 1-18.

Domalski, E.S., Milne T.A., (eds.) 1987. Thermodynamic Data for Biomass Materials and Waste Components. The ASME Research Committee on Industrial and Municipal Wastes, New York: The American Society of Mechanical Engineers.

Fischer, C.R., Klein-Marcuschamer, D., Stephanopoulos, G., 2008. Selection and optimization of microbial hosts for biofuel production. Metabolic Engineering 10, 295-304.

Florenzano, G., Poulain, M., 1984. A study of acetate production from cellulose using *Clostridium thermocellum*. Biomass 4, 295-303.

Gaddy J.L., Arora, D.K., Ko, C.W., Phillips, J.R., Basu, R., Wikstrom, C., Clausen, .E.C., 2007. Methods of increasing the production of ethanol from microbial fermentation. U.S. Patent 7 285 402 B2.2007.

Genthner, B.R.S., Bryant, M.P., 1987. Additional characteristics of one-carbon-compound utilization by *Eubacterium limosum* and *Acetobacterium woodii*. Applied and Environmental Microbiology 53, 471-476.

Gnansounou, E., 2010. Production and use of lignocellulosic bioethanol in Europe: Current situation and prospective. Bioresource Technology 101, 4842-4850.

Grethlein, A. J., Jain, M.K., 1993. Bioprocessing of coal-derived synthesis gases by anaerobic bacteria. Trends in Biotechnology 10, 418-423.

Grethlein, A.J., Jain, M.K., 1992. Bioprocessing of coal-derived synthesis gas by anaerobic bacteria. Focus, Trends in Biotechnology 10, 418-423

Grethlein, A.J., Worden, R.M., Jain, M.K., Datta, R., 1991. Evidence for production of n-butanol from carbon monoxide by *Butyribacterium methylotrophicum*. Journal of Fermentation and Bioengineering 72(1), 85-60.

Grethlein, A.J., Worden, R.M., Jain, M.K., Datta, R., 1991. Evidence for production of n-butanol from carbon monoxide by *Butyribacterium methylotrophicum.* Journal of Fermentation and Bioengineering 72, 58-60.

Haryanto, A., Fernando, S.D., Pordesimo, L.O., Adhikari, S., 2009. Upgrading of syngas derived from biomass gasification: A thermodynamic analysis. Biomass and Bioenergy 33, 882-889.

Heiskanen, H., Virkajarvi, I., Viikari, L., 2007. The effects of syngas composition on the growth and product formation of *Butyribacterium methylotrophicum*. Enzyme and Microbial Technology 41, 362-367.

Henstra, A.M., Sipma, J., Rinzema, A., Stams, A.J.M., 2007. Microbiology of synthesis gas fermentation for biofuel production. Current Opinion in Biotechnology 18, 200-206.

Hurst, K.M., Lewis, R.S., 2010. Carbon monoxide partial pressure effects on the metabolic process of syngas fermentation. Biochemical Engineering Journal 48, 159-165.

Kim, Y. B., Lenz, R.W., 2001. Polyesters from Microorganisms. Advances in Biochemical Engineering/Biotechnology 71, 51-79.

Klasson, K. T., Ackerson, C.M.D., Clausen, E.C., Gaddy. J.L., 1992. Biological conversion of synthesis gases into fuels. International Journal of Hydrogen Energy 17 (4), 281-288.

Klasson, K.T., Ackerson, C.M.D., Clausen, E.C. Gaddy, J.L.,1990. Bioreactor design for synthesis gas fermentation. Biotechnology for the production of clean fuels 28 August, Washington, USA.

Klasson, K.T., Ackerson, C.M.D., Clausen, E.C. Gaddy, J.L., 1993. Biological conversion of coal and coal-derived synthesis gas. Fuel 72, 1673-1678.

Kluyver, A. J., Schnellen, C., 1947. On the fermentation of carbon monoxide by pure cultures of methane bacteria. Archives of Biochemistry 14(1–2), 57-70.

Knudsen, J.G., Katz, D.L., 1958. Fluid dynamics and heat transfer, McGraw-Hill, New York, NY.

Kopke, M., Mihalcea, C., Bromley, J.C., Simpson, S.D. 2011. Fermentative production of ethanol from carbon monoxide. Current Opinion in Biotechnology 22, 320-325.

Krumholz, L.R., Bryant, M.P., 1985. *Clostridium pfennigii* sp. nov. uses methoxyl groups of monobenzenoids and produces butyrate. International Journal of Systematic Bacteriology 35, 454-456.

Kundiyana, D.K., Huhnke, R.L., Wilkins, M.R., 2010. Syngas fermentation in a 100-L pilot scale fermentor: Design and process considerations. Journal of Biosciences and Bioengineering 109 (5), 492-498.

Kundu, S., Premer, S. A., Hoy, J. A., Trent, J. T., Hargrove, M. S., 2003. Direct measurements of equilibrium constants for high-affinity hemoglobins. Biophysics Journal 84 (6), 3931-3940.

Lee, K.C., Rittmann, B.E., 2001. Applying a novel autohydrogenotrophic hollow-fiber membrane biofilm reactor for denitrification of drinking water. Water Research 36, 2040-2052.

Lee, S.K., Chou, H., Ham, T.S., Lee, T.S., Keasling, J.D., 2008. Metabolic engineering of microorganisms for biofuels production: from bugs to synthetic biology to fuels. Current Opinion in Biotechnology 19, 1-8.

Liou, J.S.C., Balkwill, D.L., Drake, G.R., Tanner, R.S., 2005. *Clostridium carboxidivorans* sp. nov., a solvent-producing clostridium isolated from an agricultural settling lagoon, and reclassification of the acetogen *Clostridium scatologenes* strain SL1 as *Clostridium drakei* sp. nov. International Journal of Systematic and Evolutionary Microbiology 55, 2085-2091.

Lorowitz, W.H., Bryant, M.P., 1984. *Peptostreptococcus productus* strain that grows rapidly with CO as the energy source. Applied and Environmental Microbiology 47, 961-964.

Lynd, L., Kerby, R., Zeikus, J.G., 1982. Carbon monoxide metabolism of the methylotrophic acidogen *Butyribacterium methylotrophicum*. Journal of Bacteriology 149, 255-263.

Lynd, L.R., 2008. Energy biotechnology; Editorial overview. Current opinion in Biotechnology 19, 199-201.

Mackaluso, J.D., 2007. The use of syngas derived from biomass and waste products to produce ethanol and hydrogen. Microbiology and Molecular Genetics 445 Basic Biotechnology eJournal 3, 98-103.

Madigan, M.T., Martinko, J.M., Parker J., 1997. Biology of Microorganisms, Edn 8. Edited by Brock T.D. New Jersey, Prentice-Hall, Inc.

McKendry, P., 2002. Energy production from biomass (part 1): Overview of biomass. Bioresource Technology 83 (1), 37-46.

Mohammadi, M., Najafpour, G.D., Younesi, H., Lahijani, P., Uzir, M.H., Mohamed, A. R., 2011. Bioconversion of synthesis gas to second generation biofuels: A review. Renewable and Sustainable Energy Reviews 15, 4255-4273.

Najafpour, G., Younesi, H., 2006. Ethanol and acetate synthesis from waste gases using batch culture of *Clostridium ljungdahlii*. Enzyme and Microbial Technology 38, 223-228.

Nerenberg, R., Rittmann, B.E., 2004. Hydrogen-based, hollow-fiber membrane biofilm reactor for reduction of perchlorate and other oxidized contaminants. Water Science and Technology 49, 223-230.

O'Brien, J.M., Wolkin, R.H., Moench, T.T., Morgan, J.B., Zeikus, J.G., Lupton, F.S., Conrad, R., 1984. Association of hydrogen metabolism with unitrophic or mixotrophic growth of *Methanosarcina barkeri* on carbon monoxide. Journal of Bacteriology 158, 373-375.

Parshina, S.N., Sipma, J., Nakashimada, Y., Henstra, A.M., Smidt, H., Lysenko, A.M., Lens, P.N.L., Lettinga, G., Stams, A.J.M., 2005. *Desulfotomaculum*

carboxidivorans sp. nov., a novel sulfate-reducing bacterium capable of growth at 100% CO. International Journal of Systematic and Evolutionary Microbiology 55, 2159-2165.

Phillips, J.R., Clausen, E.C., Gaddy, J.L., 1994. Synthesis gas as substrate for the biological production of fuels and chemicals. Applied Biochemistry and Biotechnology 45-46, 145-157.

Ragauskas, A.J., Williams, C.K., Davison, B.H., Britovsek, G., Cairney, J., Eckert, C.A. et al., 2006. The path forward for biofuels and biomaterials. Science 311, 484-489.

Ragsdale, S.W., Pierce, E., 2008. Acetogenesis and the Wood-Ljundahl pathway of CO(2) fixation. Biochimica et Biophysica Acta 1784, 1873-1898.

Rajagopalan, S., Datar, R.P., Lewis, R.S., 2002. Formation of ethanol from carbon monoxide via a new microbial catalyst. Biomass and Bioenergy 23, 487-493.

Ravinder, T., Swamy, M.V., Seenayya, G., Reddy, G., 2001. *Clostridium lentocellum SG6*-a potential organism for fermentation of cellulose to acetic acid. Bioresource Technology 80, 171-177.

Riggs, S. S., Heindel, T. J., 2006. Measuring carbon monoxide gas-liquid mass transfer in a stirred tank reactor for syngas fermentation. Biotechnology Progress *22* (3), 903-906.

Rother, M., Metcalf, W.W., 2004. Anaerobic growth of *Methanosarcina acetivorans* C2A on carbon monoxide: an unusual way of life for a methanogenic archaeon. Process Natural Academy of Science USA 101,16929-16934.

Savage, M.D., Wu, Z.G., Daniel, S.L., Lundie, L.L., Drake, H.L., 1987. Carbon monoxide-dependent chemolithotrophic growth of *Clostridium thermoautotrophicum.* Applied Environmental Microbiology 53, 1902-1906.

Shen, G.J., Shieh, J.S., Grethlein, A.J., Jain, M.K., Zeikus J.H., 1999. Biochemical basis for carbon monoxide tolerance and butonol production by *Butyribacterium methylotrophicum*. Applied Microbial Biotechnology 51, 827-832.

Sim, J.H., Kamaruddin, A.H., Long, W.S., Najafpour, G., 2007. *Clostridium aceticum* – A potential organism in catalyzing carbon monoxide to acetic acid: Application of

response surface methodology. Enzyme and Microbial Technology 40, 1234–1243.

Sipma, J., Henstra, A. M., Parshina, S. N., Lens, P. N. L., Lettinga, G., Stams, A. J. M., 2006. Microbial CO conversions with applications in synthesis gas purification and biodesulfurization. Critical Reviews in Biotechnology 26 (1), 41-65.

Sipma, J., Lens, P.N.L., Stams, A.J.M., Lattinga, G., 2003. Carbon monoxide conversion by araerobic bioreactor sludges. FEMS Microbiology Ecology 44, 271-277.

Slepova, T.V., Sokolova, T.G., Lysenko, A.M., Tourova, T.P., Kolganova, T.V., Kamzolkina, O.V., Karpov, G.A., Bonch-Osmolovskaya, E.A., 2006. *Carboxydocella sporoproducens* sp. nov., a novel anaerobic CO-utilizing/H_2-producing thermophilic bacterium from a Kamchatka hot spring. International Journal of Systematic and Evolutionary Microbiology 56,797-800.

Smith, F.L., Harvey, A.H., 2007. Avoid Common Pitfalls When Using Henry's Law. Chemical Engineering Progress (ISSN 0360-7275).

Stelmachowski, M., Nowicki, L., 2003. Fuel from the synthesis gas – the role of process engineering. Applied Energy 74, 85-93.

Subramani, V., Gangwal, S.K., 2008. A review of recent literature to search for an efficient catalytic process for the conversion of syngas to ethanol. Energy Fuels 22, 814-839.

Tanner, R.S., Miller, L.M., Yang, D., 1993. *Clostridium ljungdahlii* sp. nov., an acetogenic species in clostridial ribosomal-RNA homology group-I. International Journal of Systematic Bacteriology 43, 232-236

Turn, S.Q., Kinoshita, C.M., Jakeway, L.A., Jenkins, B.M., Baxter, L.L., Wu, B.C., Blevins, L.G., 2003. Fuel characteristics of processed, high-fiber sugarcane. Fuel Processing Technology 81, 35-55.

van Kasteren, J.M.N., 2006. Co-gasification of wood and polythene with the aim of CO and H_2 production. Journal of Master Cycles and Waste Management 8, 95-98.

Vega, J.L., Clausen, E.C., Gaddy, J.L., 1990. Design of Bioreactors for Coal Synthesis Gas Fermentation. Conservation and Recycling 3, 149-160.

Voss, M.A., Ahmed, T., Semmens, M.J., 1999. Long term performance of parallel flow bubbleless hollow fiber membrane aerator. Water Environmental Research 71 (1), 23-30.

Wickramasinghe, S.R., Semmens, M.J., Cussler, E.L., 1992. Mass transfer in various hollow fiber geometries. Journal of Membrane Science 69, 235-250.

Wilhelm, E., Battino, R., Wilcock, R.J., 1977. Low-pressure solubility of gases in liquid water. Chemical Review 77, 219-262.

Wood, H.G., 1992. Life with CO or CO_2 and H_2 as a source of carbon and energy. The Journal of the Federation of American Societies for Experimental Biology 5, 156-163.

Worden, R. M., Grethlein, A.J., Zeikus, J.G., Datta, R., 1989. Applied Biochemistry and Biotechnology 20/21: 687-698.

Worden, R.M., Grethlein, A.J., Jain, M.K., Datta, R., 1991. Production of butanol and ethanol from synthesis gas via fermentation. Fuel 70 (5), 615-619.

Yang, M.C., Cussler, E.L., 1986. Designing hollow fiber contactors. American Institute of Chemical Engineers Journal 32, 1910-1916.

Yoneda, N., Kusano, S., Yasui, M., Pujado, P., Wilcher, S., 2001. Recent advances in processes and catalysts for the production of acetic acid. Applied Catalysis A: General 221, 253-265.

Younesi, H., Najafpour, G., Mohameda, A.R., 2005. Ethanol and acetate production from synthesis gas via fermentation processes using anaerobic bacterium, *Clostridium ljungdahlii*. Biochemical Engineering Journal 27, 110-119.

Younesi, H., Najafpour, G., Ismail, K.S.K., Mohamed, A.R., Kamaruddin, A.H., 2008. Biohydrogen production in a continuous stirred tank bioreactor from synthesis gas by anaerobic photosynthetic bacterium: *Rhodopirillum rubrum*. Bioresource Technology 99, 2612-2619.

Zigova, J., Sturdik, E., Vandak, D., Schlosser, S., 1999. Butyric acid production by *Clostridium butyricum* with integrated extraction and pertraction. Process Biochemistry 34, 835-843.